DISEASES AND DISORDERS

Glycolysis in hepatic stellate cells coordinates fibrogenic extracellular vesicle release spatially to amplify liver fibrosis

Shalil Khanal[1], Yuanhang Liu[2], Adebowale O. Bamidele[1], Alexander Q. Wixom[1,2], Alexander M. Washington[3], Nidhi Jalan-Sakrikar[1], Shawna A. Cooper[3], Ivan Vuckovic[4], Song Zhang[5], Jun Zhong[6], Kenneth L. Johnson[7], M. Cristine Charlesworth[7], Iljung Kim[8], Yubin Yeon[8], Sangwoong Yoon[9], Yung-Kyun Noh[8,9], Chady Meroueh[10], Abdul Aziz Timbilla[1,11], Usman Yaqoob[1], Jinhang Gao[1,12], Yohan Kim[13], Fabrice Lucien[13], Robert C. Huebert[1], Nissim Hay[14], Michael Simons[15], Vijay H. Shah[1], Enis Kostallari[1]*

Liver fibrosis is characterized by the activation of perivascular hepatic stellate cells (HSCs), the release of fibrogenic nanosized extracellular vesicles (EVs), and increased HSC glycolysis. Nevertheless, how glycolysis in HSCs coordinates fibrosis amplification through tissue zone-specific pathways remains elusive. Here, we demonstrate that HSC-specific genetic inhibition of glycolysis reduced liver fibrosis. Moreover, spatial transcriptomics revealed a fibrosis-mediated up-regulation of EV-related pathways in the liver pericentral zone, which was abrogated by glycolysis genetic inhibition. Mechanistically, glycolysis in HSCs up-regulated the expression of EV-related genes such as Ras-related protein Rab-31 (*RAB31*) by enhancing histone 3 lysine 9 acetylation on the promoter region, which increased EV release. Functionally, these glycolysis-dependent EVs increased fibrotic gene expression in recipient HSC. Furthermore, EVs derived from glycolysis-deficient mice abrogated liver fibrosis amplification in contrast to glycolysis-competent mouse EVs. In summary, glycolysis in HSCs amplifies liver fibrosis by promoting fibrogenic EV release in the hepatic pericentral zone, which represents a potential therapeutic target.

INTRODUCTION

Liver disease and cirrhosis are responsible for approximately 2 million deaths worldwide each year (*1*, *2*). Recently, massive efforts have been deployed to understand how cellular and molecular heterogeneity promotes liver fibrosis progression toward cirrhosis (*3*–*7*). This heterogeneity includes a specific hepatic stellate cell (HSC) subpopulation that drives liver fibrosis through high extracellular matrix deposition in specific zones in the liver (*5*, *6*, *8*, *9*). There are two main areas in the liver, the area around the portal tracts, named periportal, and the area around the central veins, named pericentral (*10*–*12*). Initial spatial studies of healthy livers have characterized the distinct transcriptional profiles of these zones which include markers such as the periportal cytochrome P450 family 2 subfamily F member 2 (Cyp2f2) and the pericentral Cyp2e1 (*8*, *13*, *14*). However, the spatial regulation of the pathways activated in pericentral versus periportal zones leading to liver fibrosis amplification remains poorly understood.

The progression of fibrosis toward cirrhosis is due to the activation of HSCs, which includes proliferation, migration, and myofibroblastic transdifferentiation that is mainly promoted by transforming growth factor–β (TGF-β) and platelet-derived growth factor–β (PDGF) (*15*, *16*). Initial studies have demonstrated that HSC activation is associated with metabolic reprogramming, including enhanced glucose metabolism *via* glycolysis, to meet high energy demands (*17*–*20*). However, a key question that remains unanswered in this nascent field of fibro-metabolism relates to whether and how fibrogenic growth factors activate glycolysis. It has been shown that pharmacological inhibition of glycolysis enzymes reduces liver fibrosis in vivo (*19*, *21*). Nevertheless, how glycolysis-driven metabolic reprogramming in activated HSCs coordinates downstream biological pathways spatially to amplify liver fibrosis is yet to be studied.

During liver fibrosis, HSC activation is regulated by a complex network of cellular cross-talk, including HSC-to-HSC communication (*7*, *16*, *22*, *23*). In the past decade, cell-derived nanosized particles named extracellular vesicles (EVs) have been demonstrated to be an important component of cellular cross-talk in liver homeostasis and pathogenesis (*24*–*26*). Initial insights from our previous work and others indicate that PDGF increases EV release and EVs secreted by activated HSCs promote liver fibrosis amplification (*22*, *23*, *27*, *28*). Yet, the signaling cascades governing vesicle trafficking genes involved in this phenomenon, as well as their in vivo spatial distribution that contributes to fibrosis, remain poorly characterized.

In this study, we demonstrate that HSC-specific glycolysis promoted liver fibrosis in vivo by increasing EV-related pathways in the fibrogenic pericentral area. In vitro PDGF-mediated glycolysis in HSCs enhanced the expression of vesicle trafficking-related genes

[1]Division of Gastroenterology and Hepatology, Mayo Clinic, Rochester, MN 55905, USA. [2]Department of Quantitative Health Sciences, Mayo Clinic, Rochester, MN 55905, USA. [3]Biochemistry and Molecular Biology Graduate Program, Mayo Clinic Graduate School of Biomedical Sciences, Mayo Clinic, Rochester, MN 55905, USA. [4]Metabolomics Core, Mayo Clinic, Rochester, MN 55905, USA. [5]Department of Cardiovascular Medicine, Mayo Clinic, Rochester, MN 55905, USA. [6]Department of Laboratory Medicine and Pathology, Mayo Clinic, Rochester, MN 55905, USA. [7]Proteomics Core, Mayo Clinic, Rochester, MN 55905, USA. [8]Department of Computer Science, Hanyang University, Seoul 04763, Republic of South Korea. [9]School of Computational Sciences, Korea Institute for Advanced Study, Seoul 02455, Republic of South Korea. [10]Department of Pathology, Division of Anatomic Pathology, Mayo Clinic, Rochester, MN 55905, USA. [11]Department of Medical Biochemistry, Faculty of Medicine, Hradec Kralove, Charles University, Hradec Kralove, Czech Republic. [12]Lab of Gastroenterology and Hepatology, State Key Laboratory of Biotherapy; Department of Gastroenterology, West China Hospital, Sichuan University, Chengdu, China. [13]Department of Urology, Mayo Clinic, Rochester, MN 55905, USA. [14]Department of Biochemistry and Molecular Genetics, College of Medicine, University of Illinois at Chicago, Chicago, IL 60607, USA. [15]Cardiovascular Research Center, Yale University, New Haven, CI 06510, USA.
*Corresponding author. Email: kostallari.enis@mayo.edu, enis.kostallari@gmail.com

through an epigenetic mechanism involving the acetylation of histone 3 lysine 9 (H3K9ac). These events led to an increased release of EVs enriched with fibrogenic proteins. Last, EVs from glycolysis-competent mice amplified liver fibrosis as compared to EVs from mice deficient in HSC-specific glycolysis. Our findings indicate that HSC-specific glycolysis signaling contributes in a spatially coordinated manner to the release of fibrogenic EVs to amplify liver fibrosis.

RESULTS

Down-regulation of glycolysis selectively in HSCs attenuates liver fibrosis in vivo

To study the involvement of glycolysis in liver fibrosis, we first aimed to examine the expression of glycolytic enzymes by single-cell and bulk RNA sequencing (RNA-seq). Our deposited single-cell RNA-seq (scRNA-seq) (GSE175939) (*9*) showed that the expression of several glycolytic enzymes was up-regulated in the collagen-producing HSC subpopulation (High-Col) in carbon tetrachloride (CCl_4)–mediated fibrotic livers, as compared to healthy controls and low collagen-expressing HSCs (Low-Col) (fig. S1A). These enzymes included hexokinases 1 and 2 (*Hk1* and *Hk2*), glucose transporter 1 (*Glut1*), enolase 1 (*Eno1*), phosphoglycerate kinase 1 (*Pgk1*), and glucose-6-phosphate isomerase 1 (*Gpi1*) (fig. S1A). In addition, *HK1*, *HK2*, and phosphofructokinase (*PFKFB4* and PFKP) mRNA levels were up-regulated in PDGF or TGF-β–activated human primary HSCs also in a deposited bulk RNA-seq (fig. S1B) (GSE119606) (*29*). The most significantly up-regulated among these enzymes in both mouse and human datasets was *Hk2*, the first rate-limiting enzyme during glycolysis (fig. S1, A and B). Therefore, we decided to investigate the role of glycolysis in HSCs during liver fibrosis by using a transgenic $HK2^{fl/fl}$ mouse strain (*30*, *31*). To generate a transgenic mouse model where glycolysis is selectively impaired in HSCs, PDGF receptor beta (PDGFRβ)–Cre^{ERT2} mice were crossed with $HK2^{fl/fl}$ mice to obtain $HK2^{\Delta HSC}$ offspring (Fig. 1A). We confirmed the significant reduction of *Hk2* expression in HSCs isolated from $HK2^{\Delta HSC}$ mice as compared to $HK2^{fl/fl}$ littermate controls at the mRNA level (Fig. 1B). Then, the $HK2^{fl/fl}$ littermate controls and $HK2^{\Delta HSC}$ mice were treated with olive oil or CCl_4 to induce liver fibrosis (Fig. 1A). CCl_4-treated $HK2^{fl/fl}$ littermate controls displayed increased expression of fibrosis-associated collagens at mRNA and protein levels, as compared to olive oil–treated $HK2^{fl/fl}$ controls (Fig. 1, C to F). However, collagen levels were significantly reduced in CCl_4-treated $HK2^{\Delta HSC}$ mice (Fig. 1, C to F). In contrast, CCl_4-mediated alpha–smooth muscle actin (αSMA) protein levels were not affected in $HK2^{\Delta HSC}$ mice (fig. S2A). Similar results were obtained with the heterozygous $HK2^{fl/+}$ and $HK2^{\Delta/+}$ mice (fig. S2, B to D). In addition, we aimed to understand whether glycolysis in HSCs is also important in periportal fibrosis. For this, $HK2^{fl/+}$ or $HK2^{\Delta/+}$ mice were fed with chow or 0.1% 3,5-diethoxycarbonyl-1,4-dihydrocolidine (DDC) diet for 12 days to induce periportal fibrosis. Compared to chow-fed $HK2^{fl/+}$ mice, DDC-fed $HK2^{fl/+}$ mice had increased liver fibrosis, as shown by alpha-1 type I collagen (COL1A1) immunofluorescence (IF), Western blot, and quantitative polymerase chain reaction (qPCR) (fig. S3). However, fibrosis was notably reduced in DDC-fed $HK2^{\Delta/+}$ mice, suggesting a role for HSC glycolysis in periportal fibrosis. In summary, these data suggest that activated HSCs increase the expression of glycolytic enzymes and HSC-specific glycolysis promotes liver fibrosis.

Spatial transcriptomics identifies the pericentral zone as fibrogenic during CCl_4-mediated liver fibrosis

To unveil the specific pathways regulated by HSC-specific glycolysis in the fibrotic zones that amplify liver fibrogenesis (Fig. 1), we performed spatial transcriptomics on liver sections from olive oil–treated $HK2^{fl/fl}$, CCl_4-treated $HK2^{fl/fl}$, and CCl_4-treated $HK2^{\Delta HSC}$ mice. As expected, the overall expression levels of the fibrosis-associated genes *Cola1* and *Col3a1* were up-regulated in CCl_4-treated $HK2^{fl/fl}$ mice compared to the olive oil–treated $HK2^{fl/fl}$ condition and decreased in CCl_4-treated $HK2^{\Delta HSC}$ mouse (Fig. 2A), confirming the previous results (Fig. 1). Next, following pathologist-based annotations of liver vessels, the spots were classified into pericentral or periportal (Fig. 2B). The pericentral spots clustered together and showed a distinct transcriptional profile from the periportal spots as demonstrated by the Uniform Manifold Approximation and Projection plot (Fig. 2C). The periportal cluster expressed higher levels of the periportal marker *Cyp2f2*, while the pericentral cluster expressed higher levels of the pericentral marker *Cyp2e1* (Fig. 2C) (*8*, *10*, *13*, *14*, *32*, *33*), confirming the accuracy of the spot classification and pathologist annotations. The unbiased bioinformatics analysis generated the cluster-specific conserved genes (Fig. 2D and table S1). Across all the conditions, periportal cluster was characterized by the expression of *Cyp2f2*, serine dehydratase (*Sds*), and hydroxysteroid 17-beta dehydrogenase 6 (*Hsd17b6*), while the pericentral cluster was characterized by the expression of *Cyp2e1*, serpin family A member 7 (*Serpina7*), and leukocyte cell–derived chemotaxin 2 (*Lect2*) (Fig. 2E). Last, HSC markers, decorin (*Dcn*) and reelin (*Reln*) (*8*, *9*, *14*, *34*), as well as fibrosis markers, *Col1a1* and *Col3a1*, were enriched in the pericentral cluster spots as compared to the periportal cluster spots, all conditions combined (Fig. 2F). In summary, in the CCl_4 model of liver fibrosis, the spots were classified into periportal versus pericentral clusters, where the pericentral cluster was the most enriched with HSC and fibrosis markers.

Glycolysis in HSCs up-regulates the vesicle trafficking pathway in the fibrogenic pericentral cluster during liver fibrosis

Spatial transcriptomics detected a total of 14,106 genes across the three experimental groups of mice, including olive oil–treated $HK2^{fl/fl}$, CCl_4-treated $HK2^{fl/fl}$, and CCl_4-treated $HK2^{\Delta HSC}$ mice. To understand the genes and pathways that were differentially regulated in the pericentral cluster where HSC and fibrosis markers were enriched, we performed a differentially expressed gene (DEG) analysis. The filters of adjusted *P* value lower than 0.05 and fold change (FC) higher than 1.5 were applied to the pericentral DEGs in the $HK2^{fl/fl}$ CCl_4 versus $HK2^{fl/fl}$ olive oil comparison, and adjusted *P* value lower than 0.05 to the $HK2^{\Delta HSC}$ CCl_4 versus $HK2^{fl/fl}$ CCl_4 comparison (Fig. 3A). There were 2304 genes up-regulated in CCl_4-treated $HK2^{fl/fl}$ mice and 1328 genes down-regulated in the CCl_4-treated $HK2^{\Delta HSC}$ condition, among which 636 genes were common between the two comparisons (Fig. 3A and table S2). To examine the pathways that were up-regulated by fibrosis and down-regulated when glycolysis was impaired selectively in HSCs, Gene Ontology analysis (PANTHER 2023) was performed. Molecular function analysis demonstrated that, among the pathways that were up-regulated with fibrosis and down-regulated when glycolysis was impaired in HSCs, PDGF and TGF-β receptor binding pathways were the most enriched (Fig. 3B and table S3). These data suggest that HSC-specific glycolysis is closely associated with these pathways. To find specific pathways that could promote and amplify liver fibrosis, cellular component analysis

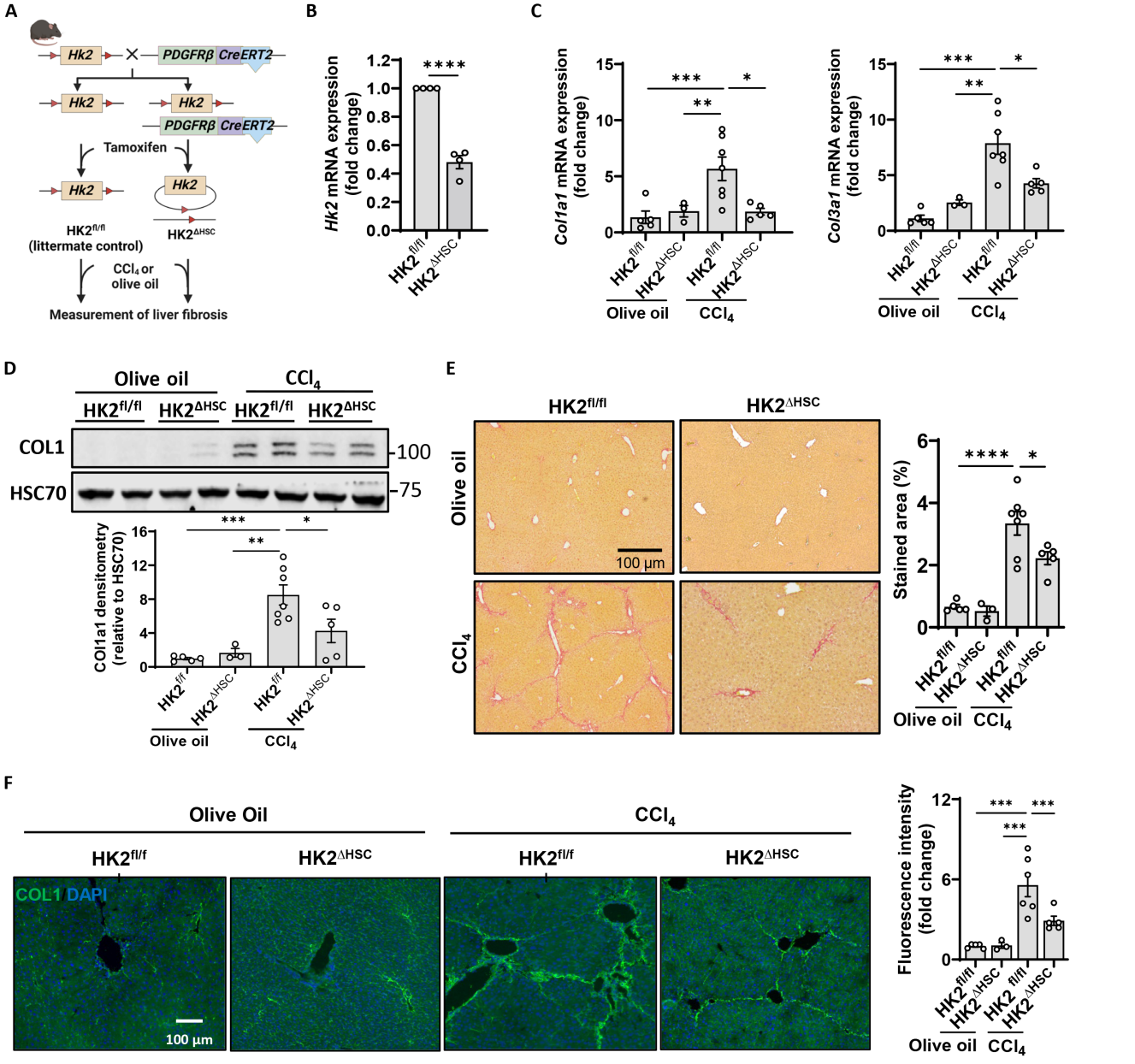

Fig. 1. Glycolytic *Hk2* deletion selectively in HSCs attenuates liver fibrosis. (**A**) Breeding schema for obtaining the HK2$^{\Delta HSC}$ mice and injury strategy for inducing liver fibrosis in these mice. Prepared with BioRender.com. (**B**) Primary mouse HSCs were isolated from HK2$^{fl/fl}$ or HK2$^{\Delta HSC}$ mice and *Hk2* mRNA levels were examined ($n = 4$, unpaired t test). (**C** to **F**) HK2$^{fl/fl}$ or HK2$^{\Delta HSC}$ male and female mice were treated with either olive oil or CCl_4 for 6 weeks. Livers were analyzed by quantitative polymerase chain reaction (qPCR) (C), Western blot (D), Sirius red (E), and Col1 immunofluorescence (F) ($n = 3$ to 7 animals per group, one-way ANOVA with Bonferroni multiple comparisons). CCl_4, carbon tetrachloride; Col1, collagen 1; HK2, hexokinase 2. Graph bars represent SEM. *$P < 0.05$, **$P < 0.01$, ***$P < 0.001$, and ****$P < 0.0001$.

was also performed. In addition to the well-established extracellular matrix–related pathways, several vesicle-related pathways, including EV-related pathways, were the most significantly enriched (Fig. 3C and table S4). We found that 176 vesicle-related genes were significantly up-regulated in fibrosis and abrogated when glycolysis was impaired selectively in HSCs (Fig. 3D). Some of the top differentially regulated genes were S100 family protein a8 (*S100a8*), *S100a9*, and Ras-related protein Rab-31 (*Rab31*) (Fig. 3, E and F), which have previously been associated with EVs (*35*–*37*). Together, these results suggest that HSC-specific glycolysis regulates PDGF, TGF-β, EV-related and extracellular matrix pathways to promote fibrosis in the pericentral areas of the liver.

Glycolysis in HSCs is stimulated by PDGF

Our spatial transcriptomics indicated that HSC-specific glycolysis correlates with PDGF and TGF-β pathways in the fibrotic pericentral zone. Thus, we first aimed to understand which growth factor promotes glycolysis in HSCs. In this regard, we performed a glycolysis

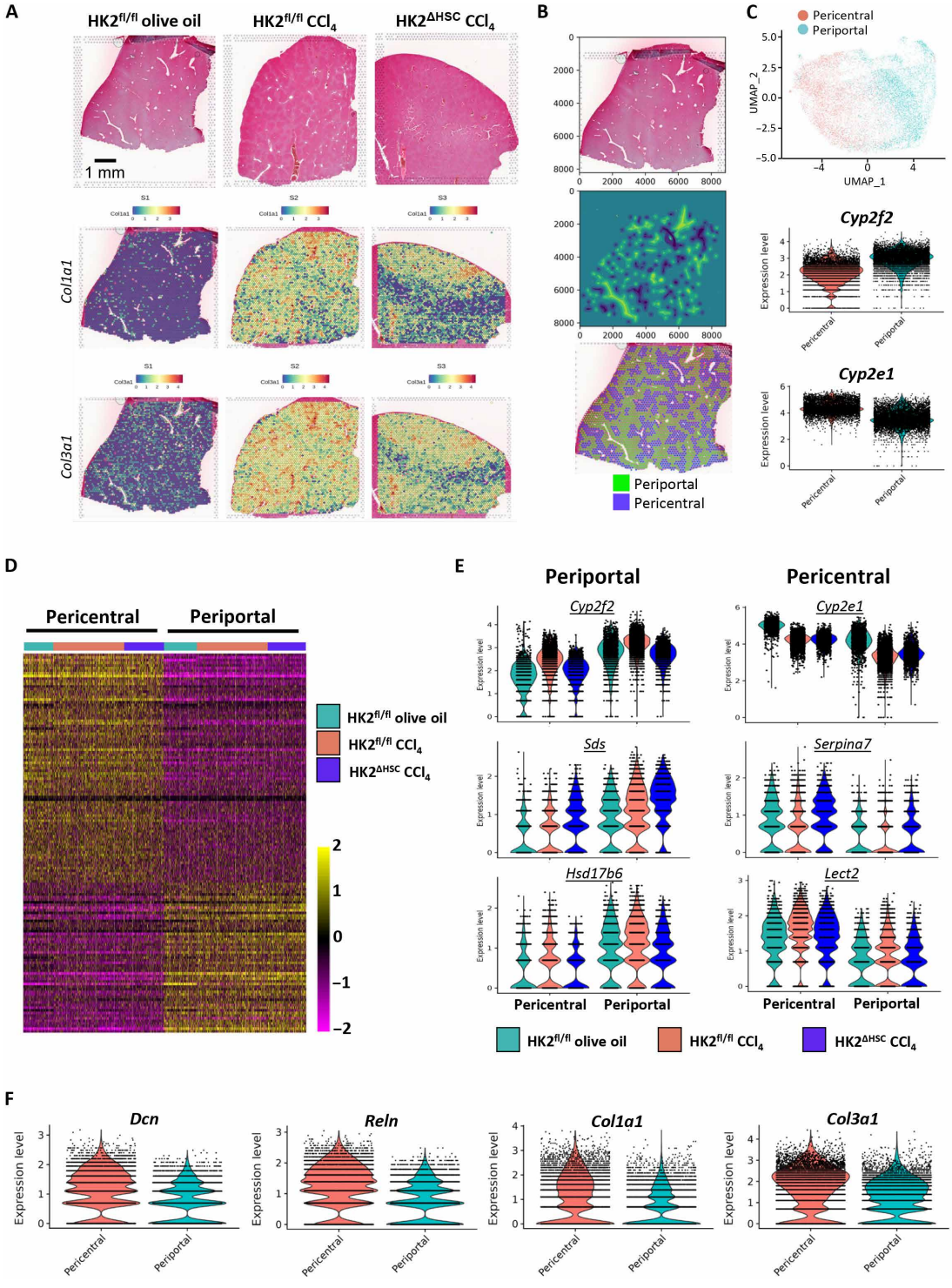

Fig. 2. Spatial transcriptomics defines two main clusters in the liver. Livers from olive oil–treated HK2$^{fl/fl}$, CCl_4-treated HK2$^{fl/fl}$, and CCl_4-treated HK2$^{\Delta HSC}$ mice were studied using 10x Genomics Spatial Transcriptomics technology. *R* package was used for statistics. (**A**) Hematoxylin and eosin of the tissues and spatial plots for *Col1a1* and *Col3a1*. (**B**) The clustering of the spots was performed based on a pathologist annotation of central and portal veins followed by a machine learning–based prediction of the clustering for each spot. (**C**) Uniform Manifold Approximation and Projection (UMAP) plot of the spots after pathologist-based clustering and violin plots of the expression of the periportal *Cyp2f2* and pericentral *Cyp2e1* markers. (**D**) Heatmap of the conserved genes in the pericentral and periportal clusters showing a distinct gene signature for each of these clusters. (**E**) Violin plots for some of the most up-regulated genes in each cluster, including *Cyp2f2*, *Sds*, and *Hsd17b6* in the periportal cluster and *Cyp2e1*, *Serpina7*, and *Lect2* in the pericentral cluster. (**F**) Violin plots of HSC markers, including *Dcn*, *Reln*, *Col1a1*, and *Col3a1*, from all conditions combined. *Col1a1*, collagen 1 alpha 1; *Col3a1*, collagen 3 alpha 1; *Cyp2e1*, cytochrome P450 family 2 subfamily E member 1; *Cyp2f2*, cytochrome P450 family 2 subfamily F member 2; *Dcn*, decorin; *Hsd17b6*, hydroxysteroid 17-beta dehydrogenase 6; *Lect2*, leukocyte cell–derived chemotaxin 2; *Reln*, reelin; *Sds*, serine dehydratase; *Serpina7*, serpin family A member 7.

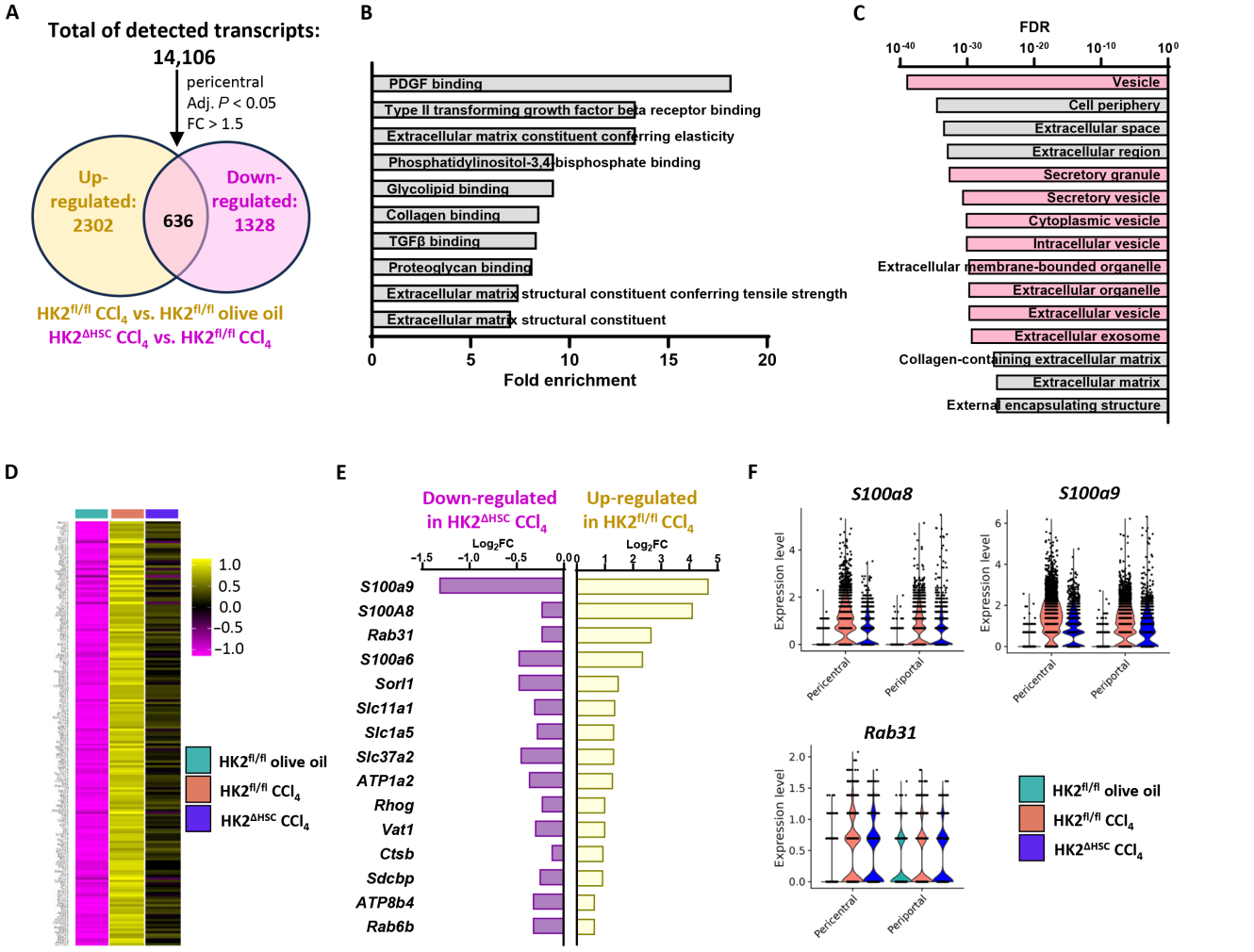

Fig. 3. Glycolysis inhibition selectively in HSCs down-regulates vesicle trafficking pathways in the fibrogenic pericentral cluster. Livers from olive oil–treated $HK2^{fl/fl}$, CCl_4-treated $HK2^{fl/fl}$, and CCl_4-treated $HK2^{\Delta HSC}$ mice were studied using 10x Genomics Spatial Transcriptomics technology. *R* package was used for statistics. (**A**) Identification of the genes in the fibrogenic pericentral cluster that were up-regulated with fibrosis ($HK2^{fl/fl}$ CCl_4 versus $HK2^{fl/fl}$ olive oil) and down-regulated when HK2 was deleted selectively in HSCs ($HK2^{\Delta HSC}$ CCl_4 versus $HK2^{fl/fl}$ CCl_4). (**B**) Gene Ontology pathway analysis of the molecular functions (Panther 2023) of the genes up-regulated with fibrosis and down-regulated with HSC-specific *Hk2* deletion. (**C**) Gene Ontology pathway analysis of the cellular components (Panther 2023) of the genes up-regulated with fibrosis and down-regulated with HSC-specific *Hk2* deletion. (**D**) Heatmap of the vesicle trafficking-related genes up-regulated with fibrosis and down-regulated with HSC-specific *Hk2* deletion. (**E**) The top genes from the vesicle trafficking and EV-related pathways that were up-regulated with fibrosis and down-regulated with HSC-specific *Hk2* deletion. (**F**) Violin plots of the top three genes from the EV-related pathways that were up-regulated with fibrosis and down-regulated with HSC-specific *Hk2* deletion.

stress test using a Seahorse analyzer, which measures in real-time the extracellular acidification rate (ECAR) reflecting the glycolytic activity and the oxygen consumption rate (OCR) indicative of the mitochondrial respiration level. Compared to vehicle, PDGF priming of primary human HSCs for 1 hour significantly increased the ECAR upon glucose (Glc) addition, which was enhanced during oligomycin (OM)-mediated the inhibition of oxidative phosphorylation (Fig. 4A). This suggests that PDGF promotes glycolysis. Furthermore, inhibiting the first rate-limiting step in glycolysis with 2-deoxyglucose (2-DG) abolished the ECAR of HSCs (Fig. 4A), thus confirming the specificity of PDGF in promoting glycolysis. However, the PDGF priming of HSCs for 1 hour did not induce any change in oxygen consumption (Fig. 4A), suggesting that PDGF might affect more glycolysis than oxidative phosphorylation. In contrast to PDGF, 1-hour TGF-β priming of HSCs did not significantly modify the ECAR, the OCR, or glucose consumption (fig. S4, A to C), leading us to investigate the role of PDGF-mediated glycolysis. Congruently, PDGF treatment of primary human HSCs increased mRNA and protein levels of the glycolytic enzyme HK2 (Fig. 4, B and C), which is in accordance with the deposited bulk RNA-seq data (GSE119606) (fig. S1B) (*29*). Congruent with these results, PDGF treatment significantly increased the concentration of lactate in the media, as demonstrated by nuclear magnetic resonance (NMR) (Fig. 4D), as well as glucose consumption from the media as indicated by the Glucose Glo assay (Fig. 4E). In summary, these results suggest that PDGF-primed, but not TGF-β–primed, HSCs display an increased glycolytic activity.

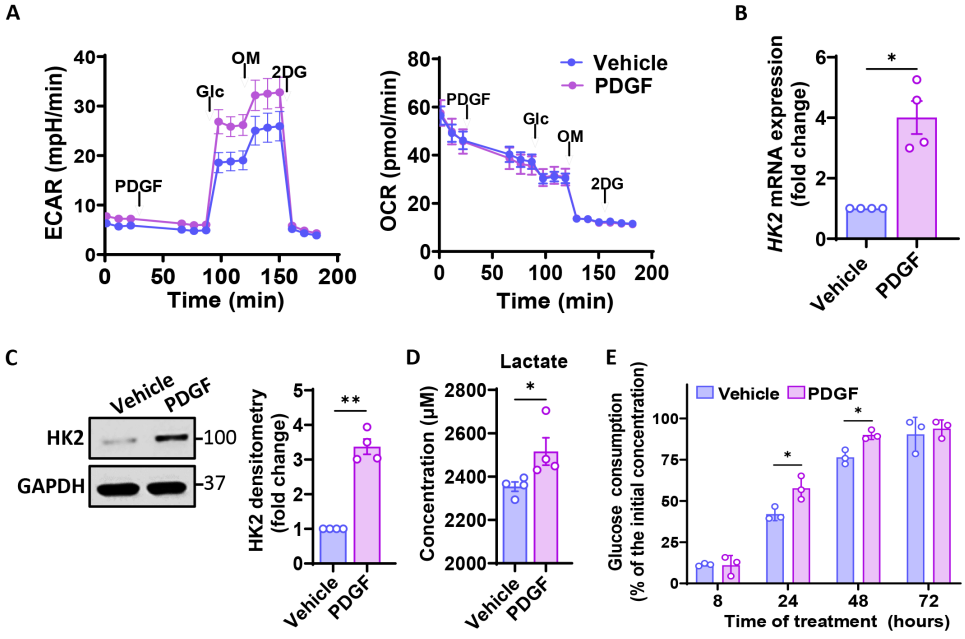

Fig. 4. Glycolysis in HSCs is stimulated by PDGF in vitro. (**A**) Seahorse glycolysis stress test measuring ECAR and OCR. Primary human HSCs, seeded at 20,000 cells per well, received direct injections of PDGF (20 ng/ml; 1 hour), 10 mM glucose (30 min), 1 μM oligomycin (30 min), and 50 mM 2-deoxyglucose (2-DG; 30 min) ($n = 3$). (**B**) Primary human HSCs were treated with vehicle or PDGF (20 ng/ml) for 4 hours and analyzed by qPCR ($n = 4$). (**C**) Primary human HSCs were treated with vehicle or PDGF (20 ng/ml) for 12 hours and analyzed by Western blot ($n = 4$). (**D**) Primary human HSCs were treated with vehicle or PDGF (20 ng/ml) for 24 hours and analyzed by nuclear magnetic resonance ($n = 4$). (**E**) Primary human HSCs were treated with vehicle or PDGF (20 ng/ml) for 8, 24, 48, or 72 hours and glucose consumption was measured ($n = 3$). Paired *t* test was used to measure the *P* value. $^*P < 0.05$ and $^{**}P < 0.01$.

PDGF-mediated glycolysis promotes the vesicle trafficking pathway in HSCs

Our spatial transcriptomics indicated that HSC-specific glycolysis promoted vesicle-related pathways (Fig. 3, C and F). Next, we sought to understand the mechanism of how PDGF-mediated glycolysis affects the vesicle trafficking pathway in HSCs. We first performed bulk RNA-seq of primary human HSCs treated in the absence or presence of glucose to induce glycolysis. The addition of glucose induced the differential expression of 918 genes (FC > 2, adjusted $P < 10^{-3}$; Fig. 5A). *Col1a1* and α*SMA* were not up-regulated by the 8-hour glucose treatment, in the absence of fibrogenic PDGF or TGF-β. Among these 918 DEGs, 107 genes were associated with the vesicle trafficking pathway (Gene Ontology identification GO:0016192) (Fig. 5A and table S5). We decided to study in more depth the role of glycolysis on vesicle trafficking-related molecules, where RAB guanosine triphosphatases (GTPases) have an essential role. The most up-regulated RAB mRNA in response to glucose was *RAB31* (Fig. 5, A and B). Furthermore, we confirmed the glucose and PDGF-mediated up-regulation of RAB31 at mRNA and protein levels by qPCR and Western blot, respectively (Fig. 5, C and D). In addition, RAB31 expression in the pericentral desmin$^+$ HSCs in CCl_4 fibrotic livers was increased when compared to olive oil control livers (fig. S5). Thus, we decided to study RAB31 as the prototype of a broader vesicle trafficking program. Consistently, *RAB31* was also identified by our spatial transcriptomics as a gene up-regulated in the pericentral zone in the fibrotic liver and down-regulated when glycolysis was impaired selectively in HSCs via *Hk2* deletion (Fig. 3, E and F). All these data suggest that RAB31 expression is regulated by glycolysis at the transcriptional level, where epigenetic marks play a crucial role. In Genome Browser (genome.ucsc.edu), the *RAB31* promoter region is associated with transcription activation marks, such as H3K9ac, histone 3 lysine 27 acetylation (H3K27ac), and histone 3 lysine 4 tri-methylation (H3K4me3) (fig. S6A). First, we investigated how PDGF-mediated glycolysis affected these activation marks by examining total protein levels. PDGF treatment of primary human HSCs increased global H3K9ac, but not H3K4me3 nor H3K27ac, which was abolished by HK2 knockdown and subsequent inhibition of glycolysis (Fig. 5E and fig. S6B). Last, chromatin immunoprecipitation (ChIP)–qPCR analysis indicated that PDGF induced a significant increase of H3K9ac specifically on the promoter region of *RAB31* (Fig. 5F) and *RAB27A* (fig. S7), another RAB protein up-regulated by glucose (Fig. 5A). Together, these results suggest that PDGF-mediated glycolysis epigenetically up-regulates the vesicle trafficking pathway in HSCs in vitro, with RAB31 as the prototype of the larger vesicle trafficking program.

PDGF-mediated glycolysis promotes EV release

RAB31 is a GTPase localized on Golgi that facilitates intracellular receptor trafficking (*38*). However, our spatial transcriptomics data indicated that glycolysis up-regulated several secretory vesicles and EV-related pathways in HSCs (Fig. 3C and table S4). Thus, we sought to investigate the noncanonical role of PDGF and glycolysis-mediated RAB31 on EV release. EVs partially originate from the intraluminal vesicles (ILVs) in the multivesicular bodies (MVBs). Thus, as a first step, we examined the effect of glycolysis on the number of ILVs per MVB. Primary human HSCs were treated in the presence of glucose, in addition to vehicle or 2-DG, the glycolysis inhibitor. Compared to vehicle, 2-DG significantly decreased the number of ILVs per MVBs, as well as the fluorescent level of the MVB marker CD63 (Fig. 6A). In

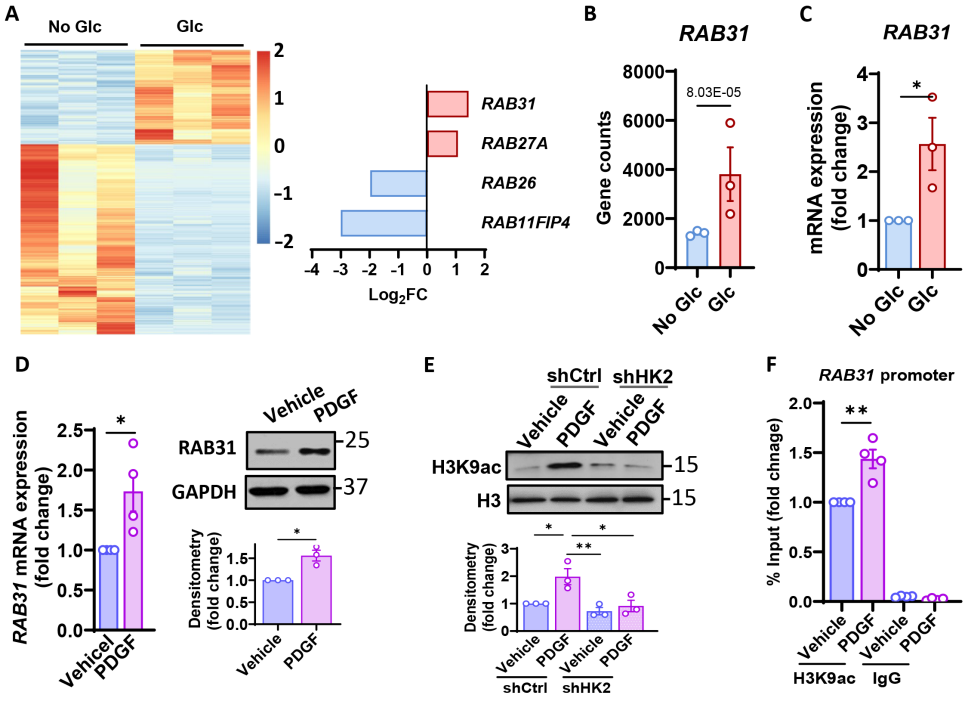

Fig. 5. PDGF-mediated glycolysis promotes the vesicle trafficking pathway through promoter region H3K9ac. (**A** and **B**) Primary human HSCs were treated in the absence (No Glc) or in the presence of glucose (Glc; 1 g/liter) for 8 hours and analyzed by bulk RNA-seq. The heatmap of the differentially expressed genes is shown and the top differentially regulated RAB genes are presented in bar graphs (A). Gene counts for the top up-regulated RAB gene, *RAB31*, are shown (B) ($n = 3$). (**C**) Primary human HSCs were treated in the absence (No Glc) or in the presence of Glc (1 g/liter) for 8 hours and *RAB31* mRNA expression was measured by qPCR ($n = 3$). (**D**) Primary human HSCs were treated with vehicle or PDGF (20 ng/ml) for 8 hours or 12 hours to measure RAB31 mRNA ($n = 4$) and protein levels ($n = 3$), respectively. (**E**) Primary human HSCs were transfected with control (shCtrl) or HK2 shRNA (shHK2), treated with either vehicle or PDGF (20 ng/ml) for 12 hours, and analyzed by Western blot ($n = 3$). Total H3 and H3K9ac were blotted simultaneously from the same samples, at the same concentration but in different lanes of the electrophoresis gel. (**F**) Primary human HSCs were treated with either vehicle or PDGF (20 ng/ml) for 12 hours. Chromatin was immunoprecipitated using an H3K9ac antibody and the *RAB31* promoter region was measured by qPCR ($n = 4$). Paired *t* test was used to measure the *P* value when comparing two groups. ANOVA with Bonferroni comparison was used to measure the *P* value when comparing more than two groups. $^*P < 0.05$ and $^{**}P < 0.01$.

addition, the presence of glucose increased the levels of the EV marker, cluster of differentiation (CD81) (*39*), in the EVs isolated from media, which was abolished when glycolysis was inhibited by 2-DG (Fig. 6B). These results suggest that glycolysis up-regulates intracellular MVB marker CD63 and extracellular EV marker CD81. Since glycolysis was increased by PDGF in HSCs (Fig. 4), we next investigated how PDGF-mediated glycolysis affects EV release. We depleted HK2 in primary human HSCs via short hairpin RNA (shRNA)–based knockdown, as confirmed at the mRNA and protein levels (Fig. 6, C and D). PDGF enhanced EV release in the media as compared to vehicle, which was abolished by HK2 knockdown, as demonstrated by CD81 protein levels and nanoparticle tracking analysis (NTA) (Fig. 6E). In addition, HK2 knockdown reduced PDGF-mediated RAB31 expression (fig. S8). Given that glycolysis affected the EV pathway and we chose RAB31 as the prototype, we next investigated the noncanonical role of RAB31 on EV release. We found that PDGF-mediated EV release was abrogated upon siRNA-mediated RAB31 knockdown, as assessed by NTA as well as nanoflow cytometry (Fig. 6, F and G). In line with these results, the EV markers, CD81 and tumor susceptibility gene 101 (TSG101), in the EV fraction from the media were increased with PDGF and abolished by RAB31 knockdown (Fig. 6H). Congruently, the inhibition of another glycolysis-dependent target RAB27A (Fig. 5A) by Nexinhib20 reduced PDGF-mediated EV release (fig. S9). Together, these results suggest that glycolysis and PDGF induce RAB-mediated EV release in HSCs.

Glycolysis-dependent EVs are fibrogenic in vitro

Our results demonstrate that glycolysis in HSCs promoted EV release (Fig. 6, B and E) and liver fibrosis (Fig. 1). Thus, we sought to examine the fibrogenic potential of glycolysis-mediated EVs. Primary human HSCs were cultured in the absence of glucose, in the presence of glucose or glucose and 2-DG. The proteomes of EVs collected from the conditioned media were subjected to tandem mass tag (TMT)–based quantitative proteomics analysis. Each protein expression was normalized to the EV marker, CD81. From a total of 1328 proteins detected in the EVs, 98 of them were differentially expressed across the three conditions (FC > 1.5, reporter intensity > 10,000) and, thus, specifically regulated by glycolysis (Fig. 7A). Compared to No Glc condition, the addition of glucose in the media modified EV cargo by increasing the content of fibrogenic proteins, such as TGF-β–induced protein (*40*, *41*), EGF-like repeats and discoidin domains 3 (EDIL3) (*42*), methionine adenosyl-transferase 2A (MAT2A) (*43*), collagens 1α1, 1α2, 6α1, 6α2, and 6α3 (Fig. 7A). Gene Ontology analysis showed that the pathways related to collagen, the main component of the extracellular matrix during liver fibrosis, are the most enriched ones in the proteins up-regulated by glucose and down-regulated by 2-DG (Fig. 7B). To

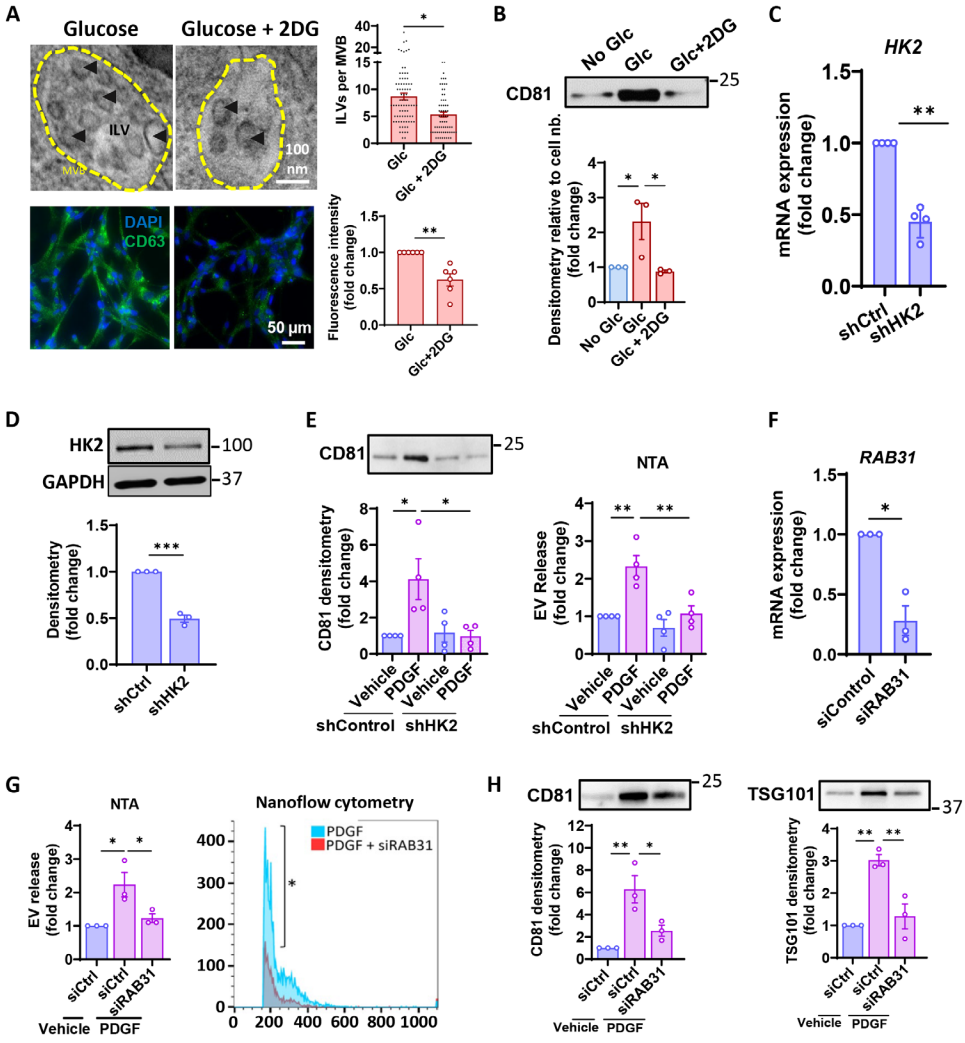

Fig. 6. PDGF-mediated glycolysis promotes EV release through RAB31. (**A**) Primary human HSCs were treated in the presence of Glc (1 g/liter) with vehicle or 2-DG for 12 hours and analyzed by transmission electron microscopy ($n = 3$) or immunofluorescence for CD63 ($n = 5$). (**B**) Primary human HSCs were treated in no glucose, Glc (1 g/liter) or Glc (1 g/liter) + 2-DG (1 g/liter) for 12 hours. EVs were purified using differential ultracentrifugation and analyzed by Western blot ($n = 3$). (**C**) Primary human HSCs were transfected with control (shCtrl) or HK2 shRNA (shHK2) and analyzed by qPCR ($n = 4$). (**D**) Primary human HSCs were transfected with control (shCtrl) or HK2 shRNA (shHK2) and analyzed by Western blot ($n = 3$). (**E**) Primary human HSCs were transfected with control (shCtrl) or HK2 shRNA (shHK2) and treated with either vehicle or PDGF (20 ng/ml) for 12 hours. EVs were purified using differential ultracentrifugation and analyzed by Western blot ($n = 4$) and nanoparticle tracking analysis (NTA; $n = 4$). (**F**) Primary human HSCs were transfected with control (siControl) or RAB31 siRNA (siRAB31) and analyzed by qPCR ($n = 3$). (**G** and **H**) Primary human HSCs were transfected with control (siCtrl) or RAB31 siRNA (siRAB31) and treated with either vehicle or PDGF (20 ng/ml) for 12 hours. EVs were purified using differential ultracentrifugation and analyzed by NTA, nanoflow cytometry (G), and Western blot (H). ($n = 3$) Paired *t* test was used to measure the *P* value when comparing two groups. ANOVA with Bonferroni comparison was used to measure the *P* value when comparing more than two groups. $^*P < 0.05$, $^{**}P < 0.01$, and $^{***}P < 0.001$.

confirm the fibrogenic nature of the glycolysis-mediated EVs, recipient primary human HSCs were treated with EVs derived from either no glucose, glucose, or glucose + 2-DG–treated donor HSCs. Compared to EVs from no glucose condition (No Glc EVs), EVs from glucose-treated HSCs (Glc EVs) significantly increased the expression of fibrotic markers *αSMA*, *COL1A1*, *fibronectin*, and proliferation marker antigen Kiel 67 (*Ki67*) in recipient HSCs (Fig. 7C). However, the expression of these fibrotic markers was abolished by EVs derived from donor HSCs where glucose-induced glycolysis was inhibited by 2-DG (Glc + 2-DG EVs) (Fig. 7C). These results suggest that glycolysis-dependent EVs from donor HSCs promote the expression of activation markers, matrix genes and proliferation marker in recipient HSCs.

Glycolysis-dependent EVs amplify liver fibrosis in vivo

In this study, we demonstrate that glycolysis-mediated EVs were fibrogenic in vitro (Fig. 7, A to C) and deletion of *Hk2* selectively in HSCs attenuated liver fibrosis (Fig. 1). In addition, compared to olive oil healthy controls, pericentral HSCs progressively increased the expression of their activation markers COL1A1 and αSMA from 4- to 6-week CCl_4 treatment (fig. S10) and they colocalized with increased expression of the EV-associated proteins CD81 and RAB31 (fig. S11). Our previous study of cell specificity of EV uptake demonstrated co-localization of injected EVs with HSCs, suggesting EV uptake by this cell type (*22*). Therefore, we investigated how HSC-specific HK2 influences the fibrogenic potential of circulating EVs and how these

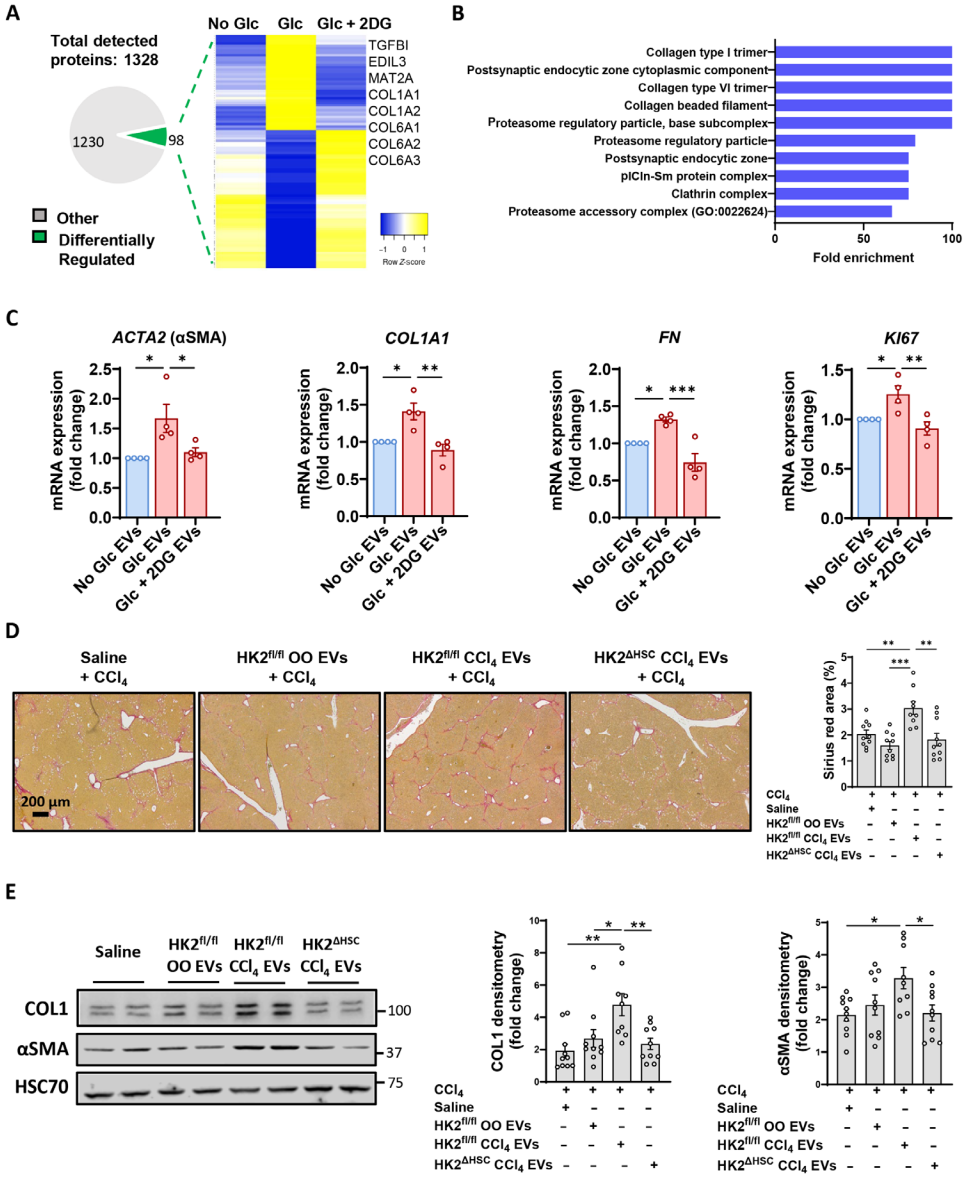

Fig. 7. Glycolysis-dependent EVs are fibrogenic in vitro and amplify liver fibrosis in vivo. (**A** and **B**) Primary human HSCs were treated in no glucose, Glc (1 g/liter), or Glc (1 g/liter) + 2-DG (1 g/liter) for 12 hours. EVs were purified using differential ultracentrifugation and analyzed by TMT-based quantitative proteomics ($n = 1$). Differentially regulated proteins among the three conditions (A) were subjected to Gene Ontology analysis using The PANTHER Classification System (www.pantherdb.org/) (B). (**C**) Donor primary human HSCs were treated in no glucose, Glc (1 g/liter), or Glc (1 g/liter) + 2-DG (1 g/liter) for 12 hours, EVs were purified from donor HSCs using differential ultracentrifugation and used to treat recipient primary human HSCs for 24 hours. Recipient HSCs were analyzed by qPCR ($n = 4$). (**D** and **E**) C57Bl/6 male and female mice were treated for 4 weeks with phosphate-buffered saline or an equal number of EVs derived from donor mice as indicated, in conjunction with CCl_4 for 4 weeks. Livers were analyzed by Sirius red (D) and Western blot (E) ($n = 9$ to 10 animals per group) ANOVA with Bonferroni comparison was used to measure the P value when comparing more than two groups. *$P < 0.05$, **$P < 0.01$, and ***$P < 0.001$.

EVs exacerbate fibrosis in vivo. To address this, donor mice, $Hk2^{fl/fl}$ littermate controls or $HK2^{\Delta HSC}$ mice, were treated with olive oil or CCl_4 for 6 weeks followed by isolation of circulating EVs. Then, saline or 2×10^8 EVs from each donor group were transplanted into recipient 8-week-old WT mice daily by intraperitoneal injections, 5 days/week in conjunction with 2 days/week CCl_4 for 4 weeks. Compared to saline administration, EVs from olive oil–treated $Hk2^{fl/fl}$ donor mice did not affect basal liver fibrosis (Fig. 7, D and E). However, EVs from CCl_4-treated $Hk2^{fl/fl}$ littermate controls significantly exacerbated liver fibrosis, as evidenced by increased Sirius red staining as well as protein levels of COL1A1 and αSMA (Fig. 7, D and E), suggesting that these EVs were fibrogenic. In contrast, EVs isolated from CCl_4-treated $HK2^{\Delta HSC}$ mice failed to amplify liver fibrosis in recipient mice (Fig. 7, D and E), suggesting that genetic inhibition of glycolysis selectively in HSCs reduced the fibrogenic potential of the circulating EVs. In summary, these results suggest that glycolysis-mediated EVs are fibrogenic and they promote liver fibrosis amplification.

DISCUSSION

In this study, by using single-cell, spatial, bulk transcriptomics, and proteomics, we demonstrate the role of HSC-specific glycolysis in spatially regulating specific pathways that govern the amplification of liver fibrosis. More specifically, we found that glycolysis in HSCs was not a consequence but a driver of liver fibrosis. In addition, we made the observation that HSC-specific glycolysis promoted EV-related gene expression in the fibrogenic pericentral zone through an epigenetic mechanism. Last, we provide evidence that glycolysis-dependent EVs amplify in vivo liver fibrosis, a mechanism in perpetuating fibrosis and liver disease (Fig. 8).

During liver fibrosis, it has been shown that HSC activation is associated with an increase in glycolytic activity (*17*, *19*, *44*, *45*). Furthermore, the pharmacological inhibition of the glycolysis enzyme phosphofructokinase reduces liver fibrosis in mice (*19*, *21*). However, the deep molecular mechanisms of how glycolysis promotes HSC activation and liver fibrosis remain poorly understood. Our scRNA-seq (*9*) data indicate that the highly fibrogenic HSC subpopulation significantly up-regulates the expression of *Hk2*, the first rate-limiting step enzyme in glycolysis. Here, we demonstrate that glycolysis inhibition through *Hk2* deletion selectively in PDGFRβ^{+} HSCs significantly reduced liver fibrogenesis in vivo, suggesting that HSC-specific glycolysis is not a consequence but a driver of fibrosis. More recently, it has been shown that HK2 promotes the canonical fibrogenic COL1A1 and αSMA expression in HSCs (*45*). Nevertheless, HK2 also has glycolysis-independent functions, such as inhibiting apoptosis, enhancing autophagy, and regulating gene transcription (*46*–*49*). In our study, 8-hour-long glucose treatment–mediated glycolysis in HSCs, in the absence of fibrogenic PDGF or TGF-β, did not increase *COL1A1* or *αSMA* mRNA expression, suggesting that HSC-specific glycolysis drives liver fibrosis through additional mechanisms, such as the release of fibrogenic EVs.

The fibrotic liver is a highly heterogeneous organ at cellular and molecular levels, with a zonally distributed metabolic gene expression (*4*, *5*). However, how HSC glycolysis drives the comprehensive molecular definitions in the fibrotic niche in the liver remains unknown. In our study, we found that HSC-specific glycolysis promoted several vesicle trafficking-related pathways, and in particular, EV-related pathways, in the fibrogenic pericentral zones. Here, we report that PDGF, but not TGF-β, increased glycolysis. We speculate that TGF-β may satisfy the energy demands during HSC transdifferentiation into myofibroblasts through other metabolic pathways. Glycolysis can regulate the epigenetic mechanism of gene expression (*50*, *51*). Recent findings show that HK2 induces histone lactylation in HSCs (*45*). In our study, we demonstrate that PDGF-mediated glycolysis promoted histone acetylation. More specifically, PDGF-mediated glycolysis in HSCs augmented EV-related gene expression, such as *RAB31* (*37*), through H3K9ac. Our findings suggest a mechanism where glycolysis in HSCs participates in liver fibrosis by increasing EV-related gene expression in the fibrogenic pericentral zone through an epigenetic mechanism.

We and others have previously reported that activated HSCs release fibrogenic EVs that amplify fibrosis (*23*, *52*). It has also been shown that glycolytic enzymes transfer into EVs and metabolic dysfunctional hepatocyte-derived EVs promote liver cancer (*53*, *54*). Nevertheless, the role of glycolysis on the content and release of HSC-derived EVs as well as how glycolysis-dependent EVs affect liver fibrosis are unknown. Here, we demonstrate that glycolysis increased the number of EVs released by HSCs and enriched these EVs with fibrogenic proteins. In addition, HSC glycolysis–dependent EVs increased recipient HSC activation and amplified in vivo liver fibrosis. These data provide a mechanism for how HSC glycolysis amplifies liver fibrosis.

In summary, glycolysis in HSCs amplifies liver fibrosis by promoting the release of fibrogenic EVs in the pericentral zones in the liver. Efficient pharmacological inhibitors of glycolysis targeting HK2 or other glycolytic enzymes are currently unexplored in the treatment of liver fibrosis in the clinic, defining an important future area of investigation for drug development. Moreover, the spatial transcriptomics dataset, in conjunction with single-cell and bulk RNA-seq datasets, can be used to identify additional targets that are up-regulated in the fibrogenic zones and activated HSCs during liver fibrosis. In conclusion, inhibition of glycolytic enzymes such as HK2 and subsequent epigenetic mechanisms might serve as a target in the treatment of liver fibrosis.

MATERIALS AND METHODS

In vivo experiments

All animal experiments were approved by the Mayo Clinic Institutional Animal Care and Use Committee. Age-matched and sex-matched mice were selected for experiments. HK2$^{fl/fl}$ mice were generated by N. Hay (*30*) and provided by M. Simons (*31*). We crossed HK2$^{fl/fl}$ with PDGFRB^{creERT2} [The Jackson Laboratory B6.Cg-Tg(Pdgfrb-cre/ERT2)6096Rha/J] mice to obtain PDGFRB^{creERT2}/Hk2$^{fl/fl}$ mice. Intraperitoneal administration of tamoxifen (75 mg/kg per day) for 5 consecutive days was used to activate Cre-ERT2 and induce HSCs-specific deletion of the Hk2 gene (HK2$^{\Delta HSC}$). There was at least a 1-week waiting period after the last tamoxifen injection before any experimentation. Liver fibrosis was induced at 8 weeks old by intraperitoneal

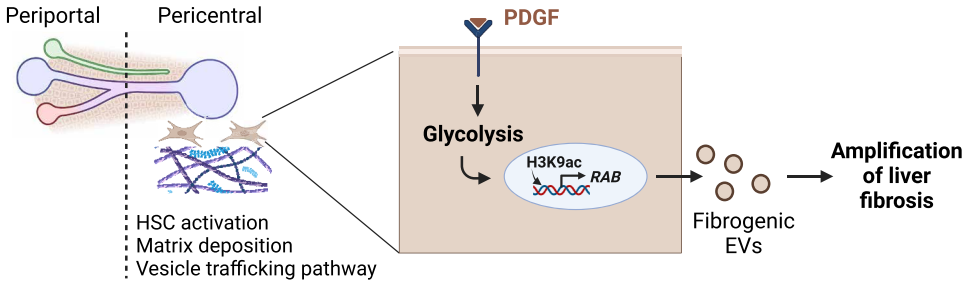

Fig. 8. Overall schema of the study. Image prepared with BioRender.com.

injection of CCl_4 (1 μl/g of body weight, Sigma-Aldrich, #319961) twice a week for 4 or 6 weeks, or by 0.1% g DDC diet for 12 days. The mice were euthanized 48 hours after the last injection. For EV transplant, EVs were isolated from the serum of olive oil or CCl_4-treated $HK2^{fl/fl}$ or $HK2^{\Delta HSC}$ mice. C57Bl/6 J wild-type recipient mice (Envigo) received intraperitoneally 2×10^8 serum EVs/mouse per day, 5 days a week for 4 weeks, in addition to CCl_4 administration twice a week. Livers were collected and analyzed by Sirius red, Western blotting (WB), qPCR, and spatial transcriptomics.

Spatial transcriptomics

Visium Technology Platform from 10x Genomics was used. Formalin-fixed paraffin-embedded (FFPE) liver sections were positioned on the capture areas of the Visium Spatial Gene Expression Slide (10x Genomics, PN-1000185) and stained with hematoxylin and eosin following the manufacturer's protocol (www.10xgenomics.com/support/spatial-gene-expression-ffpe). Liver sections were then imaged using a Huron TissueScope LE slide scanner and sequenced with NovaSeq SP at University of Minnesota Genomics Center. Only FFPE liver sections displaying a high RNA quality with total RNA fragments of more than 200 nucleotides (DV200) ranging from 64 to 71% were used. All cutoffs were calculated on the basis of the outlier detection method using the interquartile range approach. Spots with low total unique molecular identifiers counts, low number of expressed genes, high mitochondria concentration, or high hemoglobin concentration were removed. Genes detected in less than 10 spots were removed. Data were normalized using SCTransform v2 (*55*) and integrated using Harmony algorithm v0.1.1 (*56*). Clusters were determined on the basis of pathology zonation annotations from hematoxylin and eosin staining of the sections. On the basis of the contour annotations for the anatomical shapes of the central vein and portal tract, the area between the central vein and portal tract was divided into five nonoverlapping zones. These zones were arranged in order of increasing distance from the central vein to the portal tract. A nonlinear boundary between different zones was acquired using a nonlinear regression showing the anatomical distance to the boundary annotations of both the central vein and portal tract. A Gaussian process regression was learned to predict the target value −1 on the central vein boundary contours and +1 on the portal tract boundary. A topographic map was constructed with four boundaries between zones determined by the level curve with the Gaussian process output of 0.9, 0, and +0.9. Differential expression analysis was performed with the Wilcoxon rank-sum test using the FindMarkers function from Seurat v4.2 (*57*). All analysis was performed within R v4.1.2. Gene Ontology analysis (PANTHER 2023) was used to identify enriched pathways.

Cell culture

Primary mouse HSCs were isolated from mice as previously reported (*9*, *58*) and grown in Dulbecco's modified Eagle's medium (DMEM; Life Technologies, #11965092) supplemented with 10% fetal bovine serum (FBS) and 1% penicillin/streptomycin at 37°C and 5% CO_2. Primary human HSCs (ScienCell Research Laboratories, #5300) were grown in glucose-depleted DMEM (Life Technologies, #A1443001) supplemented with glucose (1 g/liter), 10% FBS, and 1% penicillin/streptomycin at 37°C and 5% CO_2. Primary human HSCs were maintained in culture up to passage 6. Primary mouse HSCs were never passaged. Cells were treated in glucose-depleted DMEM with 1% penicillin/streptomycin supplemented or not with glucose (1 g/liter). In some experiments, cells were treated with recombinant human PDGF (20 ng/ml; Sigma-Aldrich, #P3201), recombinant human TGF-β (5 ng/ml; R&D Systems #240-B), 2-DG (1 g/liter), or 0.5 μM Nexinhib20 (R&D Systems, #6089) in glucose-depleted DMEM with glucose (1 g/liter) and 1% penicillin/streptomycin. After 8 hours of treatment, cells were processed for bulk RNA-seq. After 12 hours of treatment, the conditioned media was collected for EV purification. After 24 hours of treatment, cells were processed for NMR. In some experiments, primary human HSCs were plated in a 96-well plate (50,000 cells per well) and treated with vehicle, recombinant human PDGF (20 ng/ml) or recombinant human TGF-β (5 ng/ml). Conditioned media were collected at 8, 24, 48, and 72 hours and analyzed with Glucose Glo Assay (Promega, #J6021) to measure glucose consumption following manufacturers' protocol. In some other experiments, genes were knocked down using siRNA (Dharmacon) or shRNA (Mission Millipore Sigma) as per respective manufacturer's recommended protocol.

Bulk RNA-seq

RNA-seq was performed at the Mayo Clinic Center for Individualized Medicine Medical Genomics Facility. Primary analysis was done by the Mayo Clinic Bioinformatics Core. Read quality was assessed using FastQC (v0.11.8) and reads were then trimmed using Fastx trimmer (v0.0.14). The cleaned reads were mapped to the hg38 human genome using STAR (v2.7.9a) (*59*). The STAR-generated bam files were used for tertiary analyses using R (v4.1). DESeq2 (*60*) was used to normalize the data, and extremely lowly expressed genes were filtered from the datasets (less than 10 total counts in all samples), followed by the standard differential expression pipeline. Genes were considered significantly different with $|\log_2(FC)| > 1$ and FDR (false discovery rate) > 0.05.

Seahorse glycolysis stress test

For the Seahorse glycolysis stress test, 20,000 primary human HSCs per well were plated in an XFe96 cell culture plate and incubated overnight. The cells were then washed twice with XF media followed by incubation for 1 hour in a non-CO_2 incubator before analysis in the XFe96 Extracellular Flux Analyzer (Agilent). ECAR and OCR values were measured at the basal level and then in response to sequential injections of PDGF (20 ng/ml), 10 mM glucose, 1 μM oligomycin, an adenosine 5′-triphosphate synthase inhibitor, and 50 mM 2-DG provided with the Seahorse XF Glycolysis Stress Test kit (Agilent) according to the manufacturer's instruction.

EV purification and analysis

EVs were purified using the differential ultracentrifugation method as previously described (*22*, *23*). Briefly, equal volumes of 12-hour conditioned media or serum across experimental conditions were centrifuged for 10 min at 300*g*, 30 min at 20,000*g* (large EVs), and 2.5 hours at 120,000*g* (small EVs) using Optima XPN-80 ultracentrifuge. Small EVs, referred to as EVs in this study, were resuspended in equal volumes for NTA (NS300), WB, nanoflow cytometry (Apogee Flow Systems, Apogee A60 MicroPLUS), proteomics, or EV transplantation.

Nuclear magnetic resonance

The cell media samples were collected and centrifuged at 10,000*g* for 10 min to remove any cell debris. Then, a 400 μl aliquot of supernatant was added to a 100 μl of 0.25 M phosphate buffer (pH 7.4) and 50 μl of 1 mM TSP-d4 [3-(trimethylsilyl)propionic-2,2,3,3-d4 acid

sodium salt; Sigma-Aldrich, USA] solution in D_2O. The mixture was vortexed for 20 s and transferred to a 5-mm NMR tube. After the removal of the culture medium, cells in the culture dish were washed three times with saline; 300 μl of 6% perchloric acid ($HClO_4$) was added into each culture dish, which was then flash-frozen by rapid immersion in liquid nitrogen. Frozen cells were then scraped from the culture dishes while kept on ice, transferred into 1.5-ml EP tubes, frozen in liquid nitrogen, and stored in a–80°C freezer. On the day of sample processing, frozen cells were thawed on ice, sonicated briefly then centrifuged at 10,000*g* for 10 min at 4°C. Then, 50 μl of 2 M potassium bicarbonate ($KHCO_3$; cooled to 4°C) was added to each sample. The mixed contents were then sat on ice for 15 min and centrifuged at 10,000*g* for 10 min at 4°C. A 400 μl of neutralized cell extract was added to 100 μl of phosphate buffer (pH 7.4) and 50 μl of 1 mM TSP-d4 solution in D_2O. The mixture was vortexed for 20 s and transferred to a 5-mm NMR tube. The NMR analysis was performed on a Bruker 600 MHz spectrometer (Bruker, Billerica, USA) equipped with a 5-mm BBI S3 probe and an automatic refrigerated sample changer (SampleJet). The sample temperature in the magnet was regulated to 298.2 ± 0.1 K with a BTO 2000 variable temperature unit. The NMR spectra were recorded using the standard 1D NOESY pulse sequence (noesygppr1d; Bruker BioSpin), with 65,536 data points, a spectral width of 8403 Hz, a mixing time of 10 ms, and a relaxation delay of 5 s. The cell media samples were acquired with 32 scans, and cell extract samples with 512 scans. The spectra processing included line broadening of 0.3 Hz and manual phase and baseline correction. The metabolite identification and quantification were carried out using Chenomx NMR Suite 8.5 software (Chenomx INC, Edmonton, CA). The TSP-d4 signal was used as a quantitative reference and chemical shape indicator.

Gene expression

RNA was isolated from cultured cells or liver tissues using the RNeasy Mini Kit (Qiagen, #74104). Reverse transcription was done using a SuperScript III kit (Invitrogen, #18080-051) with 500 ng of RNA. qPCR was performed using SYBR Green Supermix (Bio-Rad, #1725120). For all the steps, the manufacturers' protocols were followed. The primers were designed using Integrated DNA Technology and used to detect mouse HK2 (forward AGCCTCGGTTTCTCAATTTGG, reverse GACGCATGTGGTAGAGATACTG), mouse RAB31 (forward GAGTACGCTGAATCCATAGGTG, reverse CGCTGTTTCCATTTTCCTGAG), mouse COL1A1 (forward CATAAAGGGTCATCGTGGCT, reverse TTGAGTCCGTCTTTGCCAG), mouse COL3A1 (forward GAAGTCTCTGAAGCTGATGGG, reverse TTGCCTTGCGTGTTTGATATTC), mouse β-actin (forward CCTCCCTGGAGAAGAGCTATG, reverse TTACGGATGTCAACGTCACAC), mouse glyceraldehyde 3-phosphate dehydrogenase (GAPDH) (forward CTTTGTCAAGCTCATTTCCTGG, reverse TCTTGCTCAGTGTCCTTGC), human RAB31 (forward ATCTTTGGGCTGGGTTTG, reverse ATGGGCTCATTAGTGGGTAG), human COL1A1 (forward CCCCTGGAAAGAATGGAGATG, reverse TCCAAACCACTGAAACCTCTG), human αSMA (forward GATGGTGGGAATGGGACAAA, reverse GCCATGTTCTATCGGGTACTTC), human GAPDH (forward CCAGGGCTGCTTTTAACTCT, reverse GGACTCCACGACGTACTCA), human HK2 (forward GGGACAATGGATGCCTGAATG, reverse GTTACGGACAATCTCACCCAG), human KI67 (forward AAAAGAATTGAACCTGCGGAAG, reverse AGTCTTATTTTGGCGTCTGGAG), and human fibronectin (forward CCACAGTGGAGTATGTGGTTAG, reverse CAGTCCTTTAGGGCGATCAAT).

Quantitative proteomics analysis of EVs

TMT-based quantitation (*61*–*68*) was used to perform relative quantitation of the EV proteome from different samples. Briefly, dried EV from different samples were resolubilized in 50 mM triethylammonium bicarbonate (TEAB) (pH 8.0) and 5% SDS and subjected to reduction, alkylation, and in-solution trypsin digestion on a S-trap micro column, separately (ProtiFi, Fairport, NY). The resulting tryptic peptides from each sample were dried in a speed vacuum, resuspended in 100 mM TEAB, and then labeled with a TMTsixplex isobaric tag. The TMT-labeled peptides were mixed and fractionated by basic reversed-phase liquid chromatography to 36 fractions. The 36 fractions of TMT-labeled peptides were concatenated in a staggered pattern to six fractions. Each fraction of peptides was analyzed by liquid chromatography–tandem mass spectrometry on an Orbitrap Exploris 480 mass spectrometer. The acquired raw data were searched by the Andromeda algorithm (*69*) against a UniProt human protein database (ver. 2021-03) on the MaxQuant proteome analysis platform (ver. 1.6.17.0) (*70*). The TMT reporter ion intensities were used to perform relative quantitation of EV proteins from different samples.

WB analysis

Liver tissues or cells were lysed by using radioimmunoprecipitation assay lysis buffer (Thermo Fisher Scientific, #89900) with protease inhibitor cocktail (Roche, #4693159001). Ten to 20 μg of total protein of cell lysates or 30 to 50 μg of protein of liver lysates was loaded onto an SDS-PAGE gel for electrophoresis and proteins were transferred onto a nitrocellulose membrane. The membrane was blocked by 5% bovine serum albumin or 5% blotting-grade milk and then incubated overnight with a primary antibody. The signals of blots were developed and detected by using a chemiluminescence substrate (Millipore, #WBLUR0100 or Santa Cruz Biotechnology, #sc-2048). Heat shock cognate 71-kDa protein (HSC70) or GAPDH was used as the loading control and the results were quantified using ImageJ.

Immunofluorescence

Liver tissues or cells fixed with 4% paraformaldehyde and permeabilized with 0.5% Triton X-100 were blocked with 10% FBS followed by incubation with primary antibody overnight at 4°C. After incubation with fluorochrome-coupled secondary antibody and 4′,6-diamidino-2-phenylindole, IF signals were visualized by using a Zeiss LSM 780 confocal microscope, and signal intensity was quantified by Zen software.

Chromatin immunoprecipitation

The EZ-Magna ChIP HiSens kit (Millipore, #17-10461) was used for ChIP according to the manufacturer's recommended protocol. Briefly, cells were cross-linked with paraformaldehyde (1% final concentration) for 10 min followed by glycine (10 mM) incubation for 5 min, and genomic DNA was sheared by ultrasonication. IP was performed with protein A/G magnetic beads together with an antibody against, H3K9ac (Abcam, #aba4441) at 4°C for overnight. IP with nonimmune rabbit IgG (Diagenode, #C15410206) was used as the control. After the magnetic beads were precipitated and washed, DNA was pulled down by the antibodies, and the beads were eluted and collected for qPCR analysis. The results

were quantified and normalized to the corresponding input by the comparative Ct (ΔΔCt) method. ChIP-qPCR primers for human RAB31 promoters are forward CCGGAGGATGCTGCTGA and reverse CACCCCGAGAAGGCACA. ChIP-qPCR primers for human RAB27A promoters are forward AAAGTTTCCTACCCCTGATG and reverse GACAACTGCCTGGTGCTG.

Electron microscopy

Primary human HSCs were seeded at full confluency on carbon-coated glass coverslips and incubated for 2 hours (with or without glucose). After 2 hours, cells were fixed in 2.5% glutaraldehyde for 10 min and processed as per Mayo Microscopy and Cell Analysis Core Facility: First, samples were dehydrated, then critical-point dried, carbon-coated, and lastly imaged at 80 kV with an S-4700 electron microscope (Hitachi, Pleasanton, CA, USA).

Primary antibodies

Primary antibodies were used to detect αSMA (Abcam, #ab5694), CD81 (Santa Cruz Biotechnology, #sc-9158), CD63 (Santa Cruz Biotechnology, #sc-15363), collagen 1 (Southern Biotech, #1310-01), desmin (R&D Systems, #AF3844), GAPDH (Invitrogen, #AM4300), HSC70 (Santa Cruz Biotechnology, sc7298), HK2 (Cell signaling, #2867), histone H3 (Abcam, #ab1791), H3K9ac(Abcam, #ab4441), H3K27ac (Abcam, #ab4729), H3K4me3 (Abcam, #ab8580), RAB31 (Cell Signaling, #PA5-54064), and TSG101 (Santa Cruz Biotechnology, #sc-7964).

Statistics

Experiments include at least three independent biological replicates. Numerical data are expressed as means ± SEM. Analysis of variance with Bonferroni posttest [analysis of variance (ANOVA) or Kruskal-Wallis], paired parametric, or nonparametric *t* test was used to assess the statistical significance between groups as appropriate with GraphPad Prism 9 software (GraphPad Software, Inc., La Jolla, CA). A *P* value less than 0.05 was considered significant.

Supplementary Materials

This PDF file includes:

Figs. S1 to S11

Tables S1 to S5

REFERENCES AND NOTES

1. S. K. Asrani, H. Devarbhavi, J. Eaton, P. S. Kamath, Burden of liver diseases in the world. *J. Hepatol.* **70**, 151–171 (2019).
2. R. J. Wong, N. Kachru, D. J. Martinez, M. Moynihan, A. B. Ozbay, S. C. Gordon, Real-world comorbidity burden, health care utilization, and costs of nonalcoholic steatohepatitis patients with advanced liver diseases. *J. Clin. Gastroenterol.* **55**, 891–902 (2021).
3. M. Bhattacharya, P. Ramachandran, Immunology of human fibrosis. *Nat. Immunol.* **24**, 1423–1433 (2023).
4. B. Cogliati, C. N. Yashaswini, S. Wang, D. Sia, S. L. Friedman, Friend or foe? The elusive role of hepatic stellate cells in liver cancer. *Nat. Rev. Gastroenterol. Hepatol.* **20**, 647–661 (2023).
5. P. Ramachandran, K. P. Matchett, R. Dobie, J. R. Wilson-Kanamori, N. C. Henderson, Single-cell technologies in hepatology: New insights into liver biology and disease pathogenesis. *Nat. Rev. Gastroenterol. Hepatol.* **17**, 457–472 (2020).
6. S. B. Rosenthal, X. Liu, S. Ganguly, D. Dhar, M. P. Pasillas, E. Ricciardelli, R. Z. Li, T. D. Troutman, T. Kisseleva, C. K. Glass, D. A. Brenner, Heterogeneity of HSCs in a mouse model of NASH. *Hepatology* **74**, 667–685 (2021).
7. S. Wang, K. Li, E. Pickholz, R. Dobie, K. P. Matchett, N. C. Henderson, C. Carrico, I. Driver, M. Borch Jensen, L. Chen, M. Petitjean, D. Bhattacharya, M. I. Fiel, X. Liu, T. Kisseleva, U. Alon, M. Adler, R. Medzhitov, S. L. Friedman, An autocrine signaling circuit in hepatic stellate cells underlies advanced fibrosis in nonalcoholic steatohepatitis. *Sci. Transl. Med.* **15**, eadd3949 (2023).
8. R. Dobie, J. R. Wilson-Kanamori, B. E. P. Henderson, J. R. Smith, K. P. Matchett, J. R. Portman, K. Wallenborg, S. Picelli, A. Zagorska, S. V. Pendem, T. E. Hudson, M. M. Wu, G. R. Budas, D. G. Breckenridge, E. M. Harrison, D. J. Mole, S. J. Wigmore, P. Ramachandran, C. P. Ponting, S. A. Teichmann, J. C. Marioni, N. C. Henderson, Single-cell transcriptomics uncovers zonation of function in the mesenchyme during liver fibrosis. *Cell Rep.* **29**, 1832–1847.e8 (2019).
9. E. Kostallari, B. Wei, D. Sicard, J. Li, S. A. Cooper, J. Gao, M. Dehankar, Y. Li, S. Cao, M. Yin, D. J. Tschumperlin, V. H. Shah, Stiffness is associated with hepatic stellate cell heterogeneity during liver fibrosis. *Am. J. Physiol. Gastrointest. Liver Physiol.* **322**, G234–G246 (2022).
10. S. Ben-Moshe, Y. Shapira, A. E. Moor, R. Manco, T. Veg, K. Bahar Halpern, S. Itzkovitz, Spatial sorting enables comprehensive characterization of liver zonation. *Nat. Metab.* **1**, 899–911 (2019).
11. R. Manco, S. Itzkovitz, Liver zonation. *J. Hepatol.* **74**, 466–468 (2021).
12. J. Paris, N. C. Henderson, Liver zonation, revisited. *Hepatology* **76**, 1219–1230 (2022).
13. K. B. Halpern, R. Shenhav, O. Matcovitch-Natan, B. Toth, D. Lemze, M. Golan, E. E. Massasa, S. Baydatch, S. Landen, A. E. Moor, A. Brandis, A. Giladi, A. S. Avihail, E. David, I. Amit, S. Itzkovitz, Single-cell spatial reconstruction reveals global division of labour in the mammalian liver. *Nature* **542**, 352–356 (2017).
14. F. Hildebrandt, A. Andersson, S. Saarenpaa, L. Larsson, N. Van Hul, S. Kanatani, J. Masek, E. Ellis, A. Barragan, A. Mollbrink, E. R. Andersson, J. Lundeberg, J. Ankarklev, Spatial Transcriptomics to define transcriptional patterns of zonation and structural components in the mouse liver. *Nat. Commun.* **12**, 7046 (2021).
15. C. E. Dolin, G. E. Arteel, The matrisome, inflammation, and liver disease. *Semin. Liver Dis.* **40**, 180–188 (2020).
16. T. Tsuchida, S. L. Friedman, Mechanisms of hepatic stellate cell activation. *Nat. Rev. Gastroenterol. Hepatol.* **14**, 397–411 (2017).
17. Y. Chen, S. S. Choi, G. A. Michelotti, I. S. Chan, M. Swiderska-Syn, G. F. Karaca, G. Xie, C. A. Moylan, F. Garibaldi, R. Premont, H. B. Suliman, C. A. Piantadosi, A. M. Diehl, Hedgehog controls hepatic stellate cell fate by regulating metabolism. *Gastroenterology* **143**, 1319–1329.e11 (2012).
18. H. Gilgenkrantz, A. Mallat, R. Moreau, S. Lotersztajn, Targeting cell-intrinsic metabolism for antifibrotic therapy. *J. Hepatol.* **74**, 1442–1454 (2021).
19. M. Mejias, J. Gallego, S. Naranjo-Suarez, M. Ramirez, N. Pell, A. Manzano, C. Suner, R. Bartrons, R. Mendez, M. Fernandez, CPEB4 increases expression of PFKFB3 to induce glycolysis and activate mouse and human hepatic stellate cells, promoting liver fibrosis. *Gastroenterology* **159**, 273–288 (2020).
20. N. Smith-Cortinez, K. van Eunen, J. Heegsma, S. A. Serna-Salas, S. Sydor, L. P. Bechmann, H. Moshage, B. M. Bakker, K. N. Faber, Simultaneous induction of glycolysis and oxidative phosphorylation during activation of hepatic stellate cells reveals novel mitochondrial targets to treat liver fibrosis. *Cells* **9**, 2456 (2020).
21. T. Greuter, U. Yaqoob, C. Gan, N. Jalan-Sakrikar, E. Kostallari, J. Lu, J. Gao, L. Sun, M. Liu, T. S. Sehrawat, S. H. Ibrahim, K. Furuta, K. Nozickova, B. Q. Huang, B. Gao, M. Simons, S. Cao, V. H. Shah, Mechanotransduction-induced glycolysis epigenetically regulates a CXCL1-dominant angiocrine signaling program in liver sinusoidal endothelial cells in vitro and in vivo. *J. Hepatol.* **77**, 723–734 (2022).
22. J. Gao, B. Wei, T. M. de Assuncao, Z. Liu, X. Hu, S. Ibrahim, S. A. Cooper, S. Cao, V. H. Shah, E. Kostallari, Hepatic stellate cell autophagy inhibits extracellular vesicle release to attenuate liver fibrosis. *J. Hepatol.* **73**, 1144–1154 (2020).
23. E. Kostallari, P. Hirsova, A. Prasnicka, V. K. Verma, U. Yaqoob, N. Wongjarupong, L. R. Roberts, V. H. Shah, Hepatic stellate cell-derived platelet-derived growth factor receptor-alpha-enriched extracellular vesicles promote liver fibrosis in mice through SHP2. *Hepatology* **68**, 333–348 (2018).
24. E. Kostallari, S. Valainathan, L. Biquard, V. H. Shah, P. E. Rautou, Role of extracellular vesicles in liver diseases and their therapeutic potential. *Adv. Drug Deliv. Rev.* **175**, 113816 (2021).
25. G. Parthasarathy, P. Hirsova, E. Kostallari, G. S. Sidhu, S. H. Ibrahim, H. Malhi, Extracellular vesicles in hepatobiliary health and disease. *Compr. Physiol.* **13**, 4631–4658 (2023).
26. M. Whitham, B. L. Parker, M. Friedrichsen, J. R. Hingst, M. Hjorth, W. E. Hughes, C. L. Egan, L. Cron, K. I. Watt, R. P. Kuchel, N. Jayasooriah, E. Estevez, T. Petzold, C. M. Suter, P. Gregorevic, B. Kiens, E. A. Richter, D. E. James, J. F. P. Wojtaszewski, M. A. Febbraio, Extracellular vesicles provide a means for tissue crosstalk during exercise. *Cell Metab.* **27**, 237–251.e4 (2018).
27. P. Hirsova, S. H. Ibrahim, A. Krishnan, V. K. Verma, S. F. Bronk, N. W. Werneburg, M. R. Charlton, V. H. Shah, H. Malhi, G. J. Gores, Lipid-induced signaling causes release of inflammatory extracellular vesicles from hepatocytes. *Gastroenterology* **150**, 956–967 (2016).
28. R. Wang, Q. Ding, U. Yaqoob, T. M. de Assuncao, V. K. Verma, P. Hirsova, S. Cao, D. Mukhopadhyay, R. C. Huebert, V. H. Shah, Exosome adherence and internalization by hepatic stellate cells triggers sphingosine 1-phosphate-dependent migration. *J. Biol. Chem.* **290**, 30684–30696 (2015).
29. R. Martin-Mateos, T. M. De Assuncao, J. P. Arab, N. Jalan-Sakrikar, U. Yaqoob, T. Greuter, V. K. Verma, A. J. Mathison, S. Cao, G. Lomberk, P. Mathurin, R. Urrutia, R. C. Huebert,

V. H. Shah, Enhancer of zeste homologue 2 inhibition attenuates TGF-β dependent hepatic stellate cell activation and liver fibrosis. *Cell. Mol. Gastroenterol. Hepatol.* **7**, 197–209 (2019).
30. K. C. Patra, Q. Wang, P. T. Bhaskar, L. Miller, Z. Wang, W. Wheaton, N. Chandel, M. Laakso, W. J. Muller, E. L. Allen, A. K. Jha, G. A. Smolen, M. F. Clasquin, B. Robey, N. Hay, Hexokinase 2 is required for tumor initiation and maintenance and its systemic deletion is therapeutic in mouse models of cancer. *Cancer Cell* **24**, 213–228 (2013).
31. P. Yu, K. Wilhelm, A. Dubrac, J. K. Tung, T. C. Alves, J. S. Fang, Y. Xie, J. Zhu, Z. Chen, F. De Smet, J. Zhang, S. W. Jin, L. Sun, H. Sun, R. G. Kibbey, K. K. Hirschi, N. Hay, P. Carmeliet, T. W. Chittenden, A. Eichmann, M. Potente, M. Simons, FGF-dependent metabolic control of vascular development. *Nature* **545**, 224–228 (2017).
32. S. Kling, B. Lang, H. S. Hammer, W. Naboulsi, H. Sprenger, F. Frenzel, O. Potz, M. Schwarz, A. Braeuning, M. F. Templin, Characterization of hepatic zonation in mice by mass-spectrometric and antibody-based proteomics approaches. *Biol. Chem.* **403**, 331–343 (2022).
33. F. A. Rosenberger, M. Thielert, M. T. Strauss, L. Schweizer, C. Ammar, S. C. Madler, A. Metousis, P. Skowronek, M. Wahle, K. Madden, J. Gote-Schniering, A. Semenova, H. B. Schiller, E. Rodriguez, T. M. Nordmann, A. Mund, M. Mann, Spatial single-cell mass spectrometry defines zonation of the hepatocyte proteome. *Nat. Methods* **20**, 1530–1536 (2023).
34. P. Ramachandran, R. Dobie, J. R. Wilson-Kanamori, E. F. Dora, B. E. P. Henderson, N. T. Luu, J. R. Portman, K. P. Matchett, M. Brice, J. A. Marwick, R. S. Taylor, M. Efremova, R. Vento-Tormo, N. O. Carragher, T. J. Kendall, J. A. Fallowfield, E. M. Harrison, D. J. Mole, S. J. Wigmore, P. N. Newsome, C. J. Weston, J. P. Iredale, F. Tacke, J. W. Pollard, C. P. Ponting, J. C. Marioni, S. A. Teichmann, N. C. Henderson, Resolving the fibrotic niche of human liver cirrhosis at single-cell level. *Nature* **575**, 512–518 (2019).
35. M. Carrascal, A. Areny-Balaguero, E. de-Madaria, K. Cardenas-Jaen, G. Garcia-Rayado, R. Rivera, R. M. M. Mateos, I. Pascual-Moreno, M. Gironella, J. Abian, D. Closa, Inflammatory capacity of exosomes released in the early stages of acute pancreatitis predicts the severity of the disease. *J. Pathol.* **256**, 83–92 (2022).
36. C. Fenselau, S. Ostrand-Rosenberg, Molecular cargo in myeloid-derived suppressor cells and their exosomes. *Cell. Immunol.* **359**, 104258 (2021).
37. D. Wei, W. Zhan, Y. Gao, L. Huang, R. Gong, W. Wang, R. Zhang, Y. Wu, S. Gao, T. Kang, RAB31 marks and controls an ESCRT-independent exosome pathway. *Cell Res.* **31**, 157–177 (2021).
38. C. E. L. Chua, B. L. Tang, Engagement of the small GTPase Rab31 protein and its effector, early endosome antigen 1, is important for trafficking of the ligand-bound epidermal growth factor receptor from the early to the late endosome. *J. Biol. Chem.* **289**, 12375–12389 (2014).
39. J. Kowal, G. Arras, M. Colombo, M. Jouve, J. P. Morath, B. Primdal-Bengtson, F. Dingli, D. Loew, M. Tkach, C. Thery, Proteomic comparison defines novel markers to characterize heterogeneous populations of extracellular vesicle subtypes. *Proc. Natl. Acad. Sci. U.S.A.* **113**, E968–E977 (2016).
40. M. Farooq, M. Simoes Eugenio, C. Piquet-Pellorce, S. Dion, C. Raguenes-Nicol, K. Santamaria, G. H. Kara-Ali, T. Larcher, M. T. Dimanche-Boitrel, M. Samson, J. Le Seyec, Receptor-interacting protein kinase-1 ablation in liver parenchymal cells promotes liver fibrosis in murine NASH without affecting other symptoms. *J. Mol. Med.* **100**, 1027–1038 (2022).
41. K. Yang, N. Huang, J. Sun, W. Dai, M. Chen, J. Zeng, Transforming growth factor-β induced protein regulates pulmonary fibrosis via the G-protein signaling modulator 2 /Snail axis. *Peptides* **155**, 170842 (2022).
42. X. Wei, S. Zou, Z. Xie, Z. Wang, N. Huang, Z. Cen, Y. Hao, C. Zhang, Z. Chen, F. Zhao, Z. Hu, X. Teng, Y. Gui, X. Liu, H. Zheng, H. Zhou, S. Chen, J. Cheng, F. Zeng, Y. Zhou, W. Wu, J. Hu, Y. Wei, K. Cui, J. Li, EDIL3 deficiency ameliorates adverse cardiac remodelling by neutrophil extracellular traps (NET)-mediated macrophage polarization. *Cardiovasc. Res.* **118**, 2179–2195 (2022).
43. K. Wang, S. Fang, Q. Liu, J. Gao, X. Wang, H. Zhu, Z. Zhu, F. Ji, J. Wu, Y. Ma, L. Hu, X. Shen, D. Gao, J. Zhu, P. Liu, H. Zhou, TGF-β1/p65/MAT2A pathway regulates liver fibrogenesis via intracellular SAM. *EBioMedicine* **42**, 458–469 (2019).
44. J. Bates, A. Vijayakumar, S. Ghoshal, B. Marchand, S. Yi, D. Kornyeyev, A. Zagorska, D. Hollenback, K. Walker, K. Liu, S. Pendem, D. Newstrom, R. Brockett, I. Mikaelian, S. Kusam, R. Ramirez, D. Lopez, L. Li, B. C. Fuchs, D. G. Breckenridge, Acetyl-CoA carboxylase inhibition disrupts metabolic reprogramming during hepatic stellate cell activation. *J. Hepatol.* **73**, 896–905 (2020).
45. H. Rho, A. R. Terry, C. Chronis, N. Hay, Hexokinase 2-mediated gene expression via histone lactylation is required for hepatic stellate cell activation and liver fibrosis. *Cell Metab.* **35**, 1406–1423.e8 (2023).
46. C. Bao, S. Zhu, K. Song, C. He, HK2: A potential regulator of osteoarthritis via glycolytic and non-glycolytic pathways. *Cell Commun. Signal* **20**, 132 (2022).
47. J. M. Gall, V. Wong, D. R. Pimental, A. Havasi, Z. Wang, J. G. Pastorino, R. G. B. Bonegio, J. H. Schwartz, S. C. Borkan, Hexokinase regulates Bax-mediated mitochondrial membrane injury following ischemic stress. *Kidney Int.* **79**, 1207–1216 (2011).
48. J. G. Pastorino, N. Shulga, J. B. Hoek, Mitochondrial binding of hexokinase II inhibits Bax-induced cytochrome c release and apoptosis. *J. Biol. Chem.* **277**, 7610–7618 (2002).
49. V. P. Tan, S. Miyamoto, HK2/hexokinase-II integrates glycolysis and autophagy to confer cellular protection. *Autophagy* **11**, 963–964 (2015).
50. N. Takata, J. M. Miska, M. A. Morgan, P. Patel, L. K. Billingham, N. Joshi, M. J. Schipma, Z. J. Dumar, N. R. Joshi, A. V. Misharin, R. B. Embry, L. Fiore, P. Gao, L. P. Diebold, G. S. McElroy, A. Shilatifard, N. S. Chandel, G. Oliver, Lactate-dependent transcriptional regulation controls mammalian eye morphogenesis. *Nat. Commun.* **14**, 4129 (2023).
51. H. Wu, W. Liang, M. Han, Y. Zhen, L. Chen, H. Li, Y. An, Mechanisms regulating wound healing: Functional changes in biology mediated by lactate and histone lactylation. *J. Cell. Physiol.* **238**, 2243–2252 (2023).
52. A. Charrier, R. Chen, L. Chen, S. Kemper, T. Hattori, M. Takigawa, D. R. Brigstock, Exosomes mediate intercellular transfer of pro-fibrogenic connective tissue growth factor (CCN2) between hepatic stellate cells, the principal fibrotic cells in the liver. *Surgery* **156**, 548–555 (2014).
53. Q. T. Chen, Z. Y. Zhang, Q. L. Huang, H. Z. Chen, W. B. Hong, T. Lin, W. X. Zhao, X. M. Wang, C. Y. Ju, L. Z. Wu, Y. Y. Huang, P. P. Hou, W. J. Wang, D. Zhou, X. Deng, Q. Wu, HK1 from hepatic stellate cell-derived extracellular vesicles promotes progression of hepatocellular carcinoma. *Nat. Metab.* **4**, 1306–1321 (2022).
54. Z. Wang, S. Y. Kim, W. Tu, J. Kim, A. Xu, Y. M. Yang, M. Matsuda, L. Reolizo, T. Tsuchiya, S. Billet, A. Gangi, M. Noureddin, B. A. Falk, S. Kim, W. Fan, M. Tighiouart, S. You, M. S. Lewis, S. J. Pandol, D. Di Vizio, A. Merchant, E. M. Posadas, N. A. Bhowmick, S. C. Lu, E. Seki, Extracellular vesicles in fatty liver promote a metastatic tumor microenvironment. *Cell Metab.* **35**, 1209–1226.e13 (2023).
55. C. Hafemeister, R. Satija, Normalization and variance stabilization of single-cell RNA-seq data using regularized negative binomial regression. *Genome Biol.* **20**, 296 (2019).
56. I. Korsunsky, N. Millard, J. Fan, K. Slowikowski, F. Zhang, K. Wei, Y. Baglaenko, M. Brenner, P. R. Loh, S. Raychaudhuri, Fast, sensitive and accurate integration of single-cell data with Harmony. *Nat. Methods* **16**, 1289–1296 (2019).
57. Y. Hao, S. Hao, E. Andersen-Nissen, W. M. Mauck III, S. Zheng, A. Butler, M. J. Lee, A. J. Wilk, C. Darby, M. Zager, P. Hoffman, M. Stoeckius, E. Papalexi, E. P. Mimitou, J. Jain, A. Srivastava, T. Stuart, L. M. Fleming, B. Yeung, A. J. Rogers, J. M. McElrath, C. A. Blish, R. Gottardo, P. Smibert, R. Satija, Integrated analysis of multimodal single-cell data. *Cell* **184**, 3573–3587.e29 (2021).
58. I. Mederacke, D. H. Dapito, S. Affo, H. Uchinami, R. F. Schwabe, High-yield and high-purity isolation of hepatic stellate cells from normal and fibrotic mouse livers. *Nat. Protoc.* **10**, 305–315 (2015).
59. A. Dobin, C. A. Davis, F. Schlesinger, J. Drenkow, C. Zaleski, S. Jha, P. Batut, M. Chaisson, T. R. Gingeras, STAR: Ultrafast universal RNA-seq aligner. *Bioinformatics* **29**, 15–21 (2013).
60. M. I. Love, W. Huber, S. Anders, Moderated estimation of fold change and dispersion for RNA-seq data with *DESeq2*. *Genome Biol.* **15**, 550 (2014).
61. J. Li, Z. Cai, R. D. Bomgarden, I. Pike, K. Kuhn, J. C. Rogers, T. M. Roberts, S. P. Gygi, J. A. Paulo, TMTpro-18plex: The expanded and complete set of TMTpro reagents for sample multiplexing. *J. Proteome Res.* **20**, 2964–2972 (2021).
62. R. S. Nirujogi, J. D. Wright Jr., S. S. Manda, J. Zhong, C. H. Na, J. Meyerhoff, B. Benton, R. Jabbour, K. Willis, M. S. Kim, A. Pandey, J. W. Sekowski, Phosphoproteomic analysis reveals compensatory effects in the piriform cortex of VX nerve agent exposed rats. *Proteomics* **15**, 487–499 (2015).
63. G. Sathe, K. K. Mangalaparthi, A. Jain, J. Darrow, J. Troncoso, M. Albert, A. Moghekar, A. Pandey, Multiplexed phosphoproteomic study of brain in patients with Alzheimer's disease and age-matched cognitively healthy controls. *OMICS* **24**, 216–227 (2020).
64. G. Sathe, C. H. Na, S. Renuse, A. K. Madugundu, M. Albert, A. Moghekar, A. Pandey, Quantitative proteomic profiling of cerebrospinal fluid to identify candidate biomarkers for Alzheimer's disease. *Proteomics Clin. Appl.* **13**, e1800105 (2019).
65. S. Singh, M. Y. Bhat, G. Sathe, C. Gopal, J. Sharma, A. K. Madugundu, N. S. Joshi, A. Pandey, Proteomic signatures of diffuse and intestinal subtypes of gastric cancer. *Cancers* **13**, 5930 (2021).
66. A. Thompson, J. Schafer, K. Kuhn, S. Kienle, J. Schwarz, G. Schmidt, T. Neumann, R. Johnstone, A. K. Mohammed, C. Hamon, Tandem mass tags: A novel quantification strategy for comparative analysis of complex protein mixtures by MS/MS. *Anal. Chem.* **75**, 1895–1904 (2003).
67. X. Wu, L. Wang, N. A. Pearson, S. Renuse, R. Cheng, Y. Liang, D. G. Mun, A. K. Madugundu, Y. Xu, P. S. Gill, A. Pandey, Quantitative tyrosine phosphoproteome profiling of AXL receptor tyrosine kinase signaling network. *Cancers* **13**, 4234 (2021).
68. M. S. Zahari, X. Wu, S. M. Pinto, R. S. Nirujogi, M. S. Kim, B. Fetics, M. Philip, S. R. Barnes, B. Godfrey, E. Gabrielson, E. Nevo, A. Pandey, Phosphoproteomic profiling of tumor tissues identifies HSP27 Ser82 phosphorylation as a robust marker of early ischemia. *Sci. Rep.* **5**, 13660 (2015).
69. J. Cox, N. Neuhauser, A. Michalski, R. A. Scheltema, J. V. Olsen, M. Mann, Andromeda: A peptide search engine integrated into the MaxQuant environment. *J. Proteome Res.* **10**, 1794–1805 (2011).

70. J. Cox, M. Mann, MaxQuant enables high peptide identification rates, individualized p.p.b.-range mass accuracies and proteome-wide protein quantification. *Nat. Biotechnol.* **26**, 1367–1372 (2008).

Acknowledgments

Funding: This study was supported by the NIH R01 DK136511 (to E.K.); the American Association for the Study of Liver Diseases Pinnacle Research Award (to E.K.); Mayo Clinic Center for Cell Signaling in Gastroenterology (NIDDK P30 DK084567) Pilot/Feasibility Award (to E.K.); Mayo Clinic Center for Biomedical Discoveries pilot award (E.K.); Gilead Liver Scholar award (to E.K.); NIH K01 DK124358 (to A.O.B.); Mayo Clinic Proteomics Core, a shared resource of the Mayo Clinic Cancer Center (NCI P30 CA15083), Department of Laboratory Medicine and Pathology Translational Research, Innovation and Test Development Office (TRITDO) and the Center for Individualized Medicine (CIM) at Mayo Clinic Innovation award ADL0048 (to C.M.); NIH T32 DK124190 (to S.A.C.), CTSA KL2 TR002379 from the National Center for Advancing Translational Science (NCATS) (to N.J.S.); NIH R37 AA21171 (to V.H.S.); R01DK117861 (to R.C.H.); and the Spatialomics core at University of Minnesota. **Author contributions:** Conceptualization: E.K. Writing the original draft of the manuscript: S.K., Y.K., C.M., Y.-K.N., A.Q.W., and E.K. Review and editing of the manuscript: S.K., J.Z., A.A.T., S.A.C., A.M.W., C.M., V.H.S., N.H., F.L., and E.K. Investigation: S.K., U.Y., J.Z., K.L.J., I.V., A.A.T., A.O.B., A.M.W., Y.-K.N., N.J.-S., Y.K., S.Y., S.Z., F.L., J.G., M.C.C., and E.K. Methodology: S.K., I.V., M.S., A.O.B., Y.-K.N., N.J.-S., C.M., S.Y., S.Z., F.L., M.C.C., and E.K. Resources: U.Y., K.L.J., I.V., R.C.H., M.S., A.O.B., Y.-K.N., N.J.-S., V.H.S., Y.K., S.Y., N.H., S.Z., F.L., and E.K. Funding acquisition: R.C.H., A.O.B., Y.-K.N., N.J.-S., C.M., V.H.S., and E.K. Validation: S.K., J.Z., K.L.J., I.V., A.A.T., A.M.W., Y.-K.N., Y.K., S.Z., M.C.C., and E.K. Formal analysis: S.K., I.V., A.A.T., S.A.C., Y.Y., Y.L., A.M.W., Y.-K.N., I.K., A.Q.W., C.M., Y.K., S.Y., S.Z., F.L., and E.K. Visualization: S.K., A.A.T., S.A.C., Y.L., Y.-K.N., A.Q.W., C.M., Y.K., F.L., and E.K. Software: S.K., S.A.C., Y.Y., Y.L., Y.-K.N., I.K., A.Q.W., C.M., and S.Y. Data curation: S.K., Y.Y., I.K., A.Q.W., Y.K., and E.K. Project administration: S.K. and E.K. Supervision: Y.-K.N., C.M., and E.K. **Competing interests:** The authors declare that they have no competing interests. **Data and materials availability:** All data needed to evaluate the conclusions in the paper are present in the paper and/or the Supplementary Materials. Large datasets, including bulk RNA-seq (GSE261758), spatial transcriptomics (GSE259363), and TMT proteomics (PXD050337) datasets, are deposited in GEO and ProteomeXchange, respectively.

Submitted 13 December 2023
Accepted 24 May 2024
Published 28 June 2024
10.1126/sciadv.adn5228

ScienceAdvances

Glycolysis in hepatic stellate cells coordinates fibrogenic extracellular vesicle release spatially to amplify liver fibrosis

Shalil Khanal, Yuanhang Liu, Adebowale O. Bamidele, Alexander Q. Wixom, Alexander M. Washington, Nidhi Jalan-Sakrikar, Shawna A. Cooper, Ivan Vuckovic, Song Zhang, Jun Zhong, Kenneth L. Johnson, M. Cristine Charlesworth, Iljung Kim, Yubin Yeon, Sangwoong Yoon, Yung-Kyun Noh, Chady Meroueh, Abdul Aziz Timbilla, Usman Yaqoob, Jinhang Gao, Yohan Kim, Fabrice Lucien, Robert C. Huebert, Nissim Hay, Michael Simons, Vijay H. Shah, and Enis Kostallari

Sci. Adv. **10** (26), eadn5228. DOI: 10.1126/sciadv.adn5228

Science Advances (ISSN 2375-2548) is published by the American Association for the Advancement of Science. 1200 New York Avenue NW, Washington, DC 20005. The title *Science Advances* is a registered trademark of AAAS.